Astron. Astrophys. 354, 193–215 (2000)

ASTRONOMY AND ASTROPHYSICS

Fundamental parameters of Galactic luminous OB stars

IV. The upper HR diagram⋆

A. Herrero[1,2], **J. Puls**[3], **and M.R. Villamariz**[1]

[1] Instituto de Astrofísica de Canarias, 38200 La Laguna, Tenerife, Spain
[2] Departamento de Astrofísica, Universidad de La Laguna, Avda. Astrofísico Francisco Sánchez, s/n, 38071 La Laguna, Spain
[3] Universitäts-Sternwarte München, Scheinerstrasse 1, 81679 München, Germany

Received 15 June 1999 / Accepted 9 November 1999

Abstract. We present observations and analyses of seven Galactic O stars of type O6 and earlier. The analyses are carried out using NLTE plane–parallel, hydrostatic models as well as NLTE spherical models with mass-loss. With detailed calculations for the former and simulations for the latter, it is shown that the flux blocking due to UV metal lines is important for these objects, in agreement with previous studies, and the way the mechanism operates is explained. We find that the plane–parallel, hydrostatic unblanketed model atmospheres have increasing difficulties in fitting the early-type spectra of massive stars, and for 50 000 K and above a fit seems to be impossible. The gravities derived are relatively low even for the luminosity class V stars. These objects also show the mass discrepancy found in earlier studies, indicating that sphericity and mass-loss are important, even at their higher gravities. We then perform an analysis using spherical models with mass-loss. It is found that gravities should be increased by 0.1–0.25 dex, reducing, but not solving, the mass discrepancy. We show that spectroscopic masses are in better agreement with the theory of radiatively driven winds than evolutionary masses are. A helium abundance larger than solar is also obtained for most objects.

Some additional effects (partly related to present approximations) that have an influence in our analyses are studied. It is found that He II λ4200 is less sensitive to details of the model calculations than He II λ4541 and thus it is preferred for temperature determinations, with the consequence of lower effective temperatures. It is shown that the fits to He II λ4686 are improved when the upward rates of the He II resonance lines are reduced (with respect to the conventional treatment adequate for lines formed in expanding atmospheres), either by setting them in detailed balance or by artificially adding extra opacity sources that simulate line blocking. The He II blend with H_α is also affected.

Some stars of our sample have such high mass–loss rates that the derivation of gravities from the wings of Balmer lines, in particular H_γ, becomes doubtful. For the most extreme objects, the mass–loss rates needed to fit H_α are different from those needed to fit H_γ, by a maximum factor of two.

From the point of view of individual stars, we have analysed some of the most massive and luminous stars in the Milky Way. According to our analysis, three of them (Cyg OB2 #7, HD 15 570 and HD 15 558) have particularly large initial masses, close to or in excess of 100 $M_\odot$. Finally, the least luminous object in our sample, HD 5 689, could have been erroneously assigned to Cas OB7 and might be a runaway star.

Key words: stars: atmospheres – stars: early-type – stars: evolution – stars: fundamental parameters – stars: mass-loss

1. Introduction

Massive hot stars are relevant objects in many areas of astrophysics. They are the main sources of photoionization of their surrounding interstellar medium, and they contribute to the chemical and dynamical evolution of the host galaxy through their stellar winds and supernova explosions. They are also the precursors of Wolf–Rayet stars and LBVs and constitute excellent probes of evolutionary models. For these reasons, advances in our understanding of these objects have an impact on other fields of astrophysics.

In spite of all this, few attempts have been made to analyse massive O stars quantitatively. The most comprehensive study up to now has been that of Herrero et al. (1992, hereafter Paper I), who analysed 24 stars from spectral types B0 to O5. Detailed quantitative analyses of massive stars of early spectral type have been even more scarce. Conti & Frost (1977) first made a systematic analysis of the earliest spectral types, comparing with theoretical predictions by Auer & Mihalas (1972), but only for gravities of $\log g$= 4.0. Later, Kudritzki (1980) studied HD 93250, an O3 V star, using models similar to those of Auer & Mihalas (1972), and Kudritzki et al. (1983) studied the spectrum of ζ Pup and showed that the star has a low gravity (of the order of $\log g$= 3.5) and a high helium abundance (ϵ= N(He)/(N(H)+N(He))= 0.14). Kudritzki & Hummer (1990)

Send offprint requests to: A. Herrero

⋆ The INT is operated on the island of La Palma by the RGO in the Spanish Obervatorio de El Roque de los Muchachos of the Instituto de Astrofísica de Canarias.

Correspondence to: ahd@ll.iac.es

list 15 stars earlier than spectral type O6 (only three classified as supergiants), with parameters determined using the same methods. Puls et al. (1996) list 22 stars earlier than O6 in the Milky Way and the Magellanic Clouds, still taking advantage of the optical analysis, but already incorporating the effects of sphericity and mass-loss. Pauldrach et al. (1993) analysed Melnick 42 and ζ Pup, using only the UV spectrum, and Taresch et al. (1997) made a very detailed analysis of HD 93 129A using the UV and FUV spectrum. Finally, de Koter (1998) has used the UV O V line at 1371 Å to determine the temperature of very hot stars in R136a.

All these studies have revealed a number of problems in the analyses of these stars, related to our incomplete understanding of these objects. In Paper I, the so–called helium and mass discrepancies, already present in the previous literature (see Kudritzki et al. 1983; Voels et al. 1989; Groenewegen et al. 1989; Herrero et al. 1990) were shown to be systematic. These refer to the discrepancy in the values of the stellar mass and the photospheric helium abundance obtained from the analysis of the spectrum using state-of-the-art model atmospheres and evolutionary models. The explanation of these discrepancies is still unclear (for recent working directions, see Howarth 1998).

In Paper I we already noted the correlation between the mass discrepancy and the distance of the star to the Eddington limit, indicating that the plane–parallel geometry and the hydrostatic equilibrium assumption could be the reason for the low stellar masses derived. However, the use of wind techniques in the same work already indicated that the discrepancy could be reduced, but not solved, by including mass-loss and sphericity effects. This was later confirmed in an analysis of HDE 226 868 (Herrero et al. 1995), where the authors used Unified Model atmospheres to determine the mass of this star, the optical counterpart of Cygnus X–1, by combining the spectroscopic analysis with the orbital data. A similar result has been obtained by Israelian et al. (1999) in an analysis of HD 188 209. The inclusion of mass-loss and sphericity did not seem to have any effect on the helium discrepancy either (Herrero et al. 1995) in spite of the variations that strong winds could introduce in the helium profiles as compared to static, plane–parallel atmospheres (Schaerer & Schmutz 1994). One of the reasons for this weak influence was the fact that the study in Paper I was limited to spectral types of O5 or later, because it was found that above 40 000 K the neutral helium singlet and triplet lines gave different stellar parameters. Herrero (1994) suggested that this was due to the neglect of the so-called *line-blocking*, the UV background opacity due to metal lines, during the line formation calculations. Also the inclusion of microturbulence in these calculations can reduce this difference (McErlean et al. 1998; Smith & Howarth 1998; Villamariz & Herrero, in prep.).

In this paper we study a few stars of early spectral type in an attempt to cover several objectives. First, we would like to extend our sample from Paper I towards earlier spectral types and thus cover the whole region of interest in the HR diagram with plane–parallel analyses to see their complete behaviour. Although the plane–parallel models will have difficulties in explaining even the optical spectrum of these very hot stars (see Sect. 4), this first step is needed for the subsequent application of more sophisticated models, which will use the experience gained and the parameters obtained as input. An analysis of line-blocking effects is mandatory here, as it has been seen to have an influence for the higher temperatures.

Then, we will repeat the analyses using spherical models with mass-loss, and present the study of some effects that both can influence the determination of stellar parameters and that will help us to gain new insight into the physics of these stars. Having these parameters determined, we can try to establish conclusions with respect to the use of different model atmospheres and techniques for the analysis of very early spectral types. We will compare the results of the spherical models with mass-loss with those from plane–parallel, hydrostatic model atmospheres as well as with the results obtained using the somewhat approximate technique employed by Puls et al. (1996).

In Sect. 2 we present the observations. The effects of line-blocking in plane–parallel models are treated in Sect. 3 and the spectral description and plane–parallel analysis are considered in Sect. 4. Sect. 5 shows the analyses performed with spherical models with mass-loss, while Sect. 6 contains a qualitative study of some effects of interest which explain some difficulties found in the preceding section. Then we present our discussion (Sect. 7) and conclusions (Sect. 8).

2. The observations

The observations were carried out with the 2.5 m Isaac Newton Telescope at the Roque de los Muchachos Observatory on La Palma during two different observational runs, in 1991 September and 1992 August. We have observed the spectral region between 4000 and 5000 Å, and the region around H_α. The Intermediate Dispersion Spectrograph was used with the H 2400 B grid in the blue and the H 1800 V grid in the red, attached to the 235 mm camera, which resulted in spectral resolutions of 0.6 and 0.8 Å, respectively, measured on the Cu–Ar arc. The main difference between both runs was the size of the CCD detector, with a larger wavelength coverage per exposure (400 Å instead of 220 Å in the blue) during the second run. Table 1 gives the stellar identification (usually the HD number), star name, OB association to which the star belongs, spectral type and the night in which the stellar spectrum was obtained.

The reduction of the data was done following standard procedures. We used both IRAF[1]and own software developed in IDL. The latter was also used for the spectral analysis. The S/N ratio of the reduced spectra depends on the spectral range, but is usually about 200 in the H_γ region.

3. Line blocking in plane–parallel models

In Paper I we found that the He I singlet and triplet lines of O stars hotter than 40 000 K indicated different stellar parameters when

[1] The IRAF package is distributed by the National Optical Astronomy Observatories, which is operated by the Association of Universities for Research in Astronomy, Inc., under contract with the National Science Foundation

Table 1. Journal of observations. September dates refer to 1991, and August dates to 1992. The night of 9/10 August was dedicated to H_α observations. All spectral classifications are taken from Walborn (1972, 1973), except that of HD 5 689, which is taken from Garmany & Vacca (1991). Properties indicated in the last column have been taken from Mason et al. (1998)

Order	Identification	Spectral Type	Name	Assoc.	Observing nights	Notes
1	Cyg OB2 #7	O3 If*		Cyg OB2	6/7, 9/10 Aug	
2	HD 15 570	O4 If$^+$		Cas OB6	6/7/8, 9/10 Aug	
3	HD 15 629	O5 V((f))		Cas OB6	28/29 Sep; 7/8, 9/10 Aug	
4	HD 15 558	O5 III(f)		Cas OB6	28/29 Sep; 9/10 Aug	binary
5	HD 14 947	O5 If$^+$		Per OB1	28/29 Sep; 9/10 Aug	
6	HD 210 839	O6 I(n)fp	λ Cep	Cep OB2	28/29 Sep; 9/10 Aug	runaway
7	HD 5 689	O6 V		Cas OB7	8/9, 9/10 Aug	

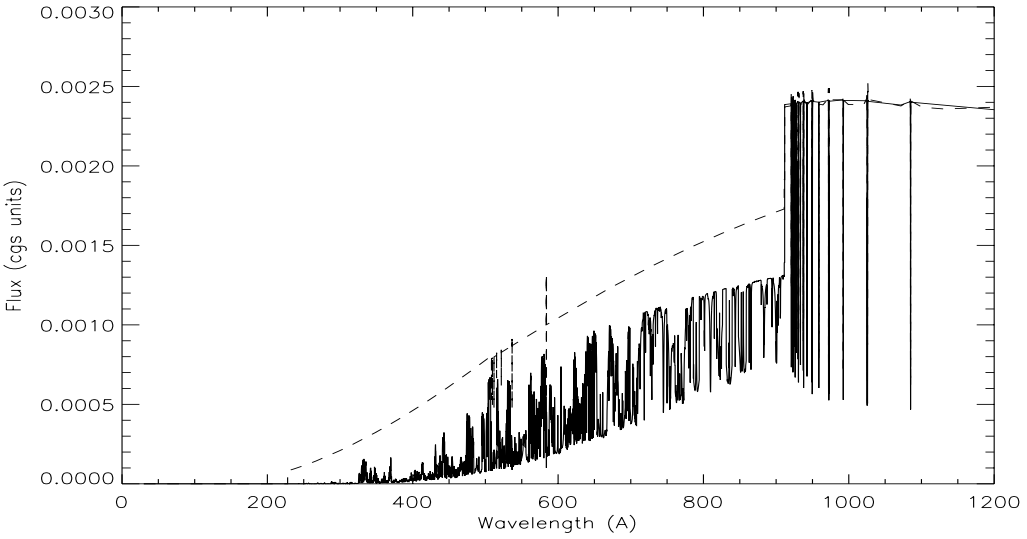

Fig. 1. The Eddington flux in the region between 228 and 1200 Å, with and without approximate line blocking, for the model at $T_{\rm eff}$ = 40 000 K, $\log g$ = 3.40 and ϵ = 0.09.

used for the determination of stellar temperatures. Following the results of Pauldrach et al. (1993), who stressed the importance of line blocking for the wind ionization structure and emergent flux, Herrero (1994) showed that this difference is considerably reduced when UV metal line opacity is included. The author attributed this to the different effect of the modified UV radiation field on the He I occupation numbers. However, no further proof was given there.

Here we want to discuss in a more detailed way the effect of this line blocking, as it is important for the analysis of the stars listed in Table 1.

We have included the line list of Pauldrach et al. (1993) between 228 and 912 Å. In this region the ionization of He I and H takes place. Thus, we can expect an effect on the occupation numbers of these two ionization stages. The line list comprises roughly 14 000 lines from 26 different elements and 137 ionization stages taken into account in the stellar wind NLTE calculations by Pauldrach et al. (1993). We calculate their occupation numbers in LTE. Although this is a rough approximation, we expect that its inclusion will already give us the major part of the effect.

We will use a model at $T_{\rm eff}$ = 40 000 K, $\log g$ = 3.40 and ϵ = 0.09 to illustrate the effects of line blocking. In Fig. 1 we plot the emergent flux between 228 and 912 Å. As we can see, a considerable fraction of the flux has been blocked. This energy will appear at other wavelengths. However, as most of the flux escapes between 912 and 2 000 Å, this has no real influence redward of 912 Å. It has to be pointed out that Fig. 1 is only illustrative. It is not the emergent flux which is important here, but the mean intensity of the radiation field at the depths where the He I continuum becomes optically thin. The effect, however, is similar.

The most important effect is produced in the occupation numbers of the ground level of He I. As a consequence of the flux blocking, the ionization from this level (its ionization edge lies at 504 Å) is considerably reduced, and its population largely increases (see Fig. 2). This does not have any noticeable effect on other ionization stages, since He I is very scarcely populated. The lower level of the He I $\lambda\lambda$4387, 4922 singlet lines, the 2p $^1P^0$ level, is directly connected to the ground level (which also belongs to the singlet system) through a radiative transition at 584 Å, and thus partially follows their changes and also increases its population. On the contrary, the lower level of the He I λ4471 triplet line (the 2p $^3P^0$ level) is only weakly or indirectly coupled to the He I ground level. In addition, the ground level of the triplet system (to which 2p $^3P^0$ is strongly coupled) is dominated by its ionization and recombination at around 2600 Å, and it is not affected by the line-blocking. As a result, the

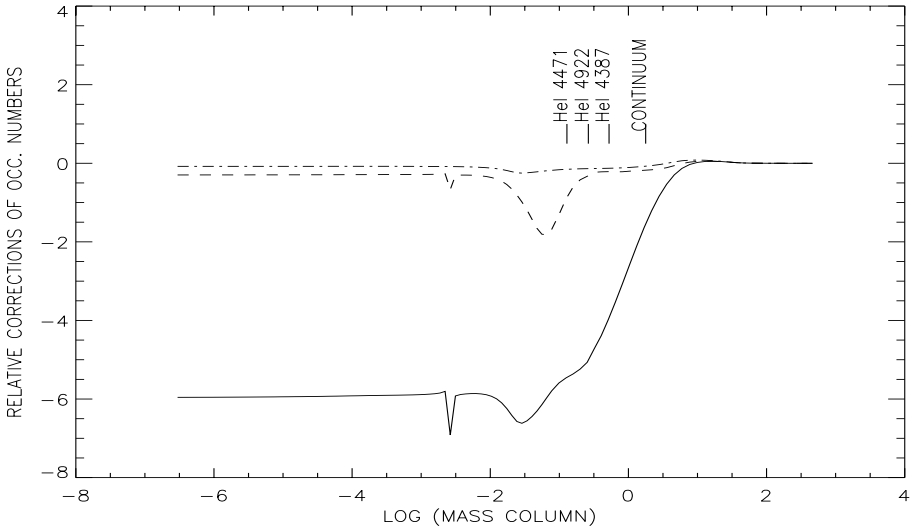

Fig. 2. The changes in the occupation numbers of the ground level of He I (full line), the lower level of the singlet lines He I $\lambda\lambda$4387, 4922 (2p $^1P^0$, dashed line) and the ground level of the triplet line He I λ4471 (2p$^3P^0$, dashed–dotted), and the formation depths of the line centers and the continuum. Negative numbers mean that the atomic level populations calculated with line-blocking are larger. The peak near log m = –2.5 is a numerical artefact in the convergence of the model without line blocking and does not appear in other models. The model parameters are the same as in Fig. 1.

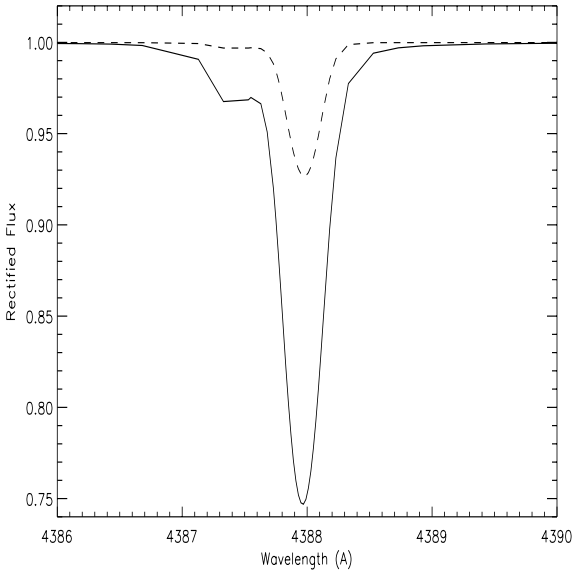

Fig. 3. The helium line He I λ4387 with and without line-blocking (solid and dashed lines, respectively) for the same model parameters as in Fig. 1. He I λ4922 behaves the same way.

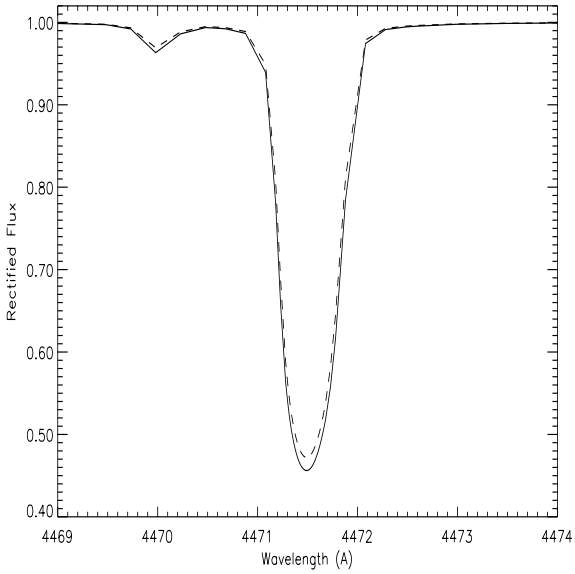

Fig. 4. As Fig. 3, but for the He I λ4471 line.

behaviour of 2p $^3P^0$ follows that of the He I ground level to a much lesser extent than does the 2p $^1P^0$ level (as do all triplet levels compared to their singlet counterparts). We can see this behaviour in Fig. 2, where we have additionally marked the formation depths of the center of the He I $\lambda\lambda$ 4387, 4922 and 4471 lines and the continuum. We can see that the populations of these levels increase over the whole region of formation, the changes being larger for the 2p $^1P^0$ level. In addition, the formation region of the singlet lines is more extended than in the case without line-blocking (an effect that is not seen in the figure). The combination of larger changes over a larger line formation region produces the stronger variations of the singlet lines compared to the triplet one.

Figs. 3 and 4 show the variations in the line profiles of He I $\lambda\lambda$4387, 4471. We see that the changes are much less in the second one, and thus this line should be preferred for analyses at high temperatures. At lower temperatures and gravities, however, and due to the so-called *dilution effect* in this line, the use of the singlet lines is preferable, even if the calculations are made without line-blocking. This effect refers to the fact that the fit of the He I λ4471 line becomes worse when going from dwarfs to supergiants, while the rest of the lines retain a good fit quality (see Voels et al. 1989). Although still not completely clarified, Smith & Howarth (1998) recently claimed that microturbulence could be the cause.

At lower temperatures or larger gravities, collisions play a stronger role, and the effects of line blocking are lower. This explains the behaviour of the corrections to the stellar parameters found by Herrero (1994, especially Fig. 3) when including line-blocking, and basically consist of obtaining lower temperatures when line-blocking is not taken into account. The amount of the correction will depend on the model temperature at a given gra-

Table 2. Parameters determined for the programme stars using plane–parallel models. Note that the parameters of Cyg OB2 #7 and HD 15 570 are only indicative, and could not be determined with the plane parallel models. Temperatures are in thousands of Kelvin. $M_{\rm s}$, $M_{\rm ev}$ and M_0 are respectively, the present spectroscopic and evolutionary masses, and the initial evolutionary mass, in solar units. The last column indicates whether we have formally a mass discrepancy considering an error of 0.22 in log($M_{\rm s}$). $V_{\rm r} \sin i$ and $v_{\rm rad}$ are given in km s^{-1}. Semicolons in $v_{\rm rad}$ indicate that the uncertainty in this value is larger than $\pm$20 kms^{-1}

Star	$v_{\rm rad}$	$T_{\rm eff}$	$\log g$	ϵ	$V_{\rm r} \sin i$	V	M_V	$R/R_\odot$	$\log(L/L_\odot)$	$M_{\rm s}$	$M_{\rm ev}$	M_0	M discr.?
Cyg OB2 #7	+35	51.0	3.66	0.12	105	–29.655	–6.20	16.7	6.23	46.2	111.8	114	Yes
HD 15 570	-20	50.0	3.51	0.15	105	–29.553	–6.73	22.0	6.44	51.1	139.1	142	Yes
HD 15 629	-50	48.0	3.81	0.09	90	–29.571	–5.52	12.7	5.89	37.5	69.9	71	Yes
HD 15 558	-35	46.5	3.71	0.07	120	–29.512	–6.28	18.5	6.16	63.8	91.7	97	No
HD 14 947	-35:	45.0	3.53	0.15	140	–29.415	–5.69	14.8	5.91	26.5	65.8	68	Yes
HD 210 839	-70	41.5	3.47	0.25	250	–29.357	–6.17	18.9	5.98	38.7	67.0	71	Yes
HD 5 689	-65	40.0	3.57	0.25	250	–29.337	–4.19	7.7	5.13	7.8	30.1	31	Yes

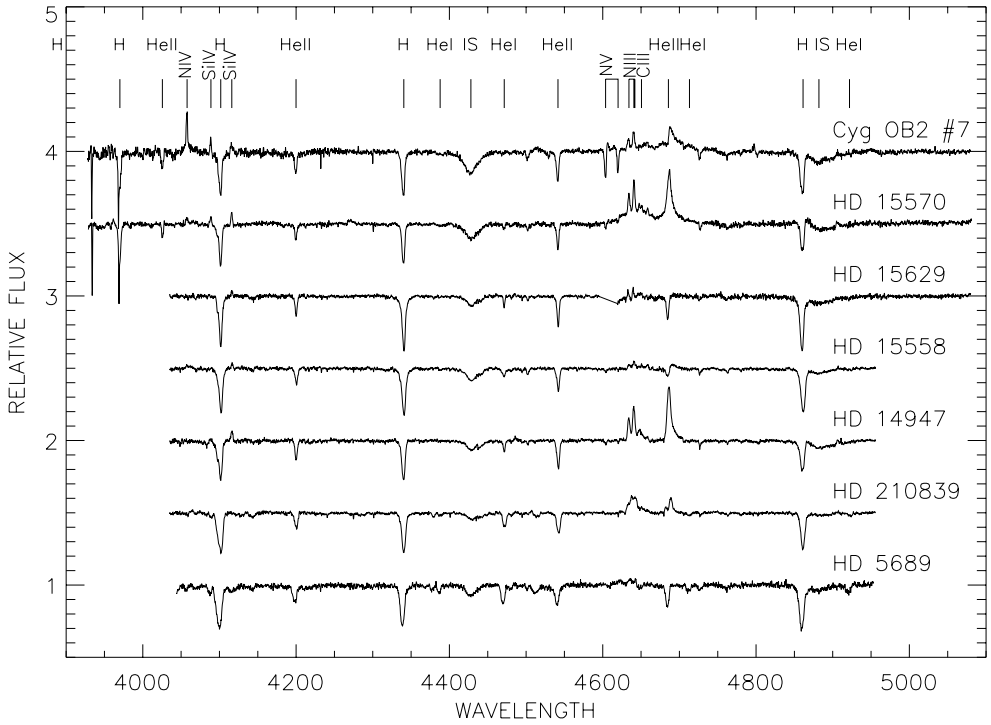

Fig. 5. The blue stellar spectra. The relative fluxes have been arbitrarily displaced in steps of 0.5 for the sake of clarity. Wavelengths are in Å.

vity, being larger for higher temperatures. It has to be stressed, however, that the corrections are large only if we use the singlet lines for the temperature determination without line–blocking. Using the triplet line results in a smaller temperature than using the singlet ones (by 500–1 000 K at temperatures around 45 000 K). Gravity and helium abundance do not significantly vary, although sometimes variations of the parameters within our typical error boxes ($\pm$0.1 in $\log g$ and $\pm$0.03 in helium abundance) have been adopted in the course of the parameter determinations.

4. Spectral analysis using plane–parallel, hydrostatic models

Fig. 5 shows the spectra of all observed stars between 4000 and 5000 Å, whereas Fig. 6 shows the spectra around H_α.

Before performing the comparison with the theoretical model atmospheres, we have corrected the spectra from radial velocity displacements. Correction for the radial velocities is crucial in the very early type stars, because the H and He lines commonly used for the spectral analysis may be contaminated by wind effects that fill their red wings. However, these corrections are particularly difficult: the cores of strong lines may be affected by the wind and only a few weak metal lines are present. Rotation adds a new handicap, as it broadens lines, making them shallower and favouring blends. In addition the limited spectral range of each single frame limits the number of suitable lines on individual spectra. Thus the first difficulty is to find a set of lines appropriate for the measurement of the radial velocity.

We have discarded all H and He lines. This is already necessary, since sometimes we can see a trend in the measured radial velocity with the excitation potential of the line, indicating that

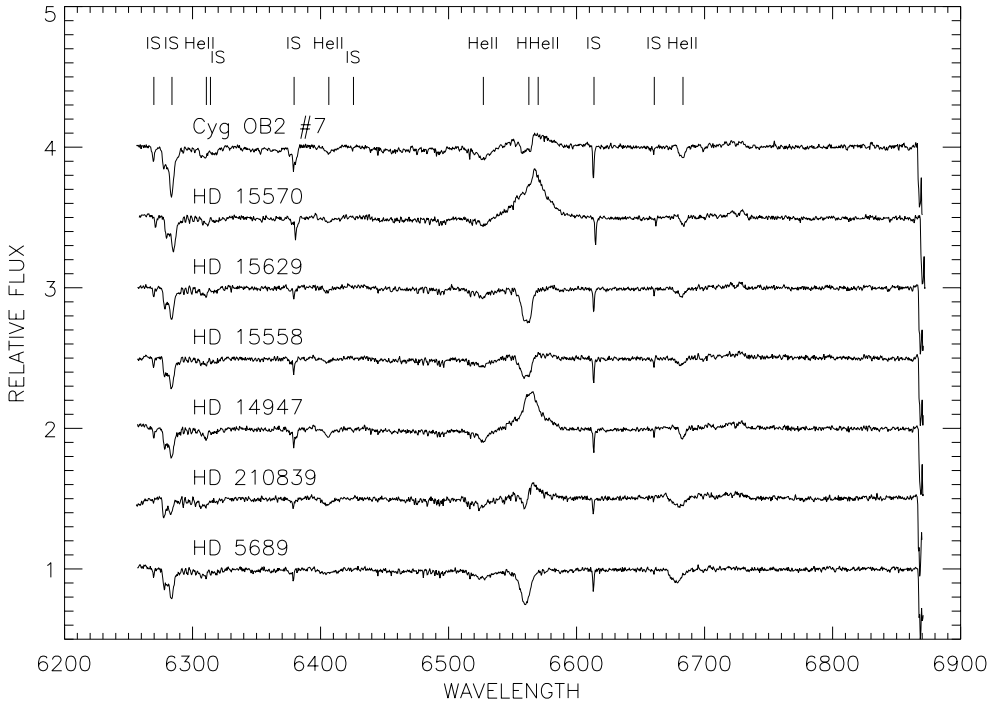

Fig. 6. As Fig. 5, however for the red spectra

the line cores are formed in higher layers moving faster as the excitation potential decreases.

Thus the radial velocity correction is based on lines of Si (Si IV and Si III), N (N V, N IV and N III), O (O II) and C (C III). Sometimes, a few lines are in emission and not in absorption. These lines are used only if they give results concordant with the rest of the metal lines (usually, this is the case). The typical uncertainties we obtain are $\pm$20 km s^{-1}, which is about half of the spectral resolution. This large error is due to the existence of only a few lines, in addition with broad cores, and reflects the dispersion in the individual values. Within these limits, we have sometimes displaced the fitted lines (also in the analysis with spherical models), when it was clear that this was the only way to obtain a good fit. Table 2 lists the radial velocities in the kinematical Local Standard of Rest.

We then determined rotational velocities following the same procedure as indicated in Paper I. Our values compare well with those by Penny (1996) and Howarth et al. (1997) for objects in common (see discussion about individual objects). Rotational velocities are given in Table 2 together with the parameters determined for each star. In this table, temperatures are given in thousands of Kelvin; gravities are corrected for centrifugal force effects (see individual discussions for model parameters); ϵ is the helium abundance by number with respect to the total number of H and He atoms; V is the integral of the stellar flux over λ, weighted by the V-filter function of Matthews & Sandage (1963), used to calculate stellar radii from the model atmospheres (see Kudritzki 1980, or Paper I); M_V is the absolute magnitude. This has been obtained using the photometry and colours from *Hipparcos* for HD 15 570, HD 15 629, HD 15 558, HD 14 947 and HD 210 839 combined with the extinction laws and distances from Garmany & Stencel (1992). For Cyg OB2 #7, M_V has been taken from Massey & Thompson (1991), and for HD 5 689 has been taken from Garmany & Stencel (1992). The evolutionary masses have been obtained from the evolutionary tracks by Schaller et al. (1992).

Except for the line-blocking, the models are the same ones used in Paper I. These are H/He,, plane–parallel models, in hydrostatic and radiative equilibrium. The line fit is also made in the same way. We first fit H$_\gamma$, obtaining the best gravity at a given $T_{\rm eff}$. The same procedure is followed for the helium lines, at a normal He abundance (i.e., 0.09 by number). The locus where all lines intersect in the log $T_{\rm eff}-\log g$ diagram is taken as giving the stellar parameters. If the lines do not intersect, the helium abundance is changed. The helium abundance giving the smallest intersection region is adopted as the one appropriate for the star. In previous studies, the helium lines used were He II $\lambda\lambda$ 4541, 4200 and He I $\lambda\lambda$ 4387, 4922, whereas He I λ 4471 was used only for dwarfs or high-temperature stars. As this is the case in the present study, this is the line we use here. In addition, for the reasons explained before, we give it a larger weight than for the singlet lines.

The errors are similar to those quoted in Paper I, with $\pm$1500 K in $T_{\rm eff}$, $\pm$0.1 in $\log g$ and $\pm$0.03 in ϵ. This produces errors of $\pm$0.06, $\pm$0.19 and $\pm$0.22 in $\log(R/R_\odot)$, $\log(M/M_\odot)$ and $\log(L/L_\odot)$, respectively, when adopting an uncertainty of $\pm$0.3 mag for M_V.

We now describe the line fits of each star independently, and the spectral features, if appropriate. In Fig. 7 we show the theoretical HR diagram for these stars, with the parameters listed in Table 2.

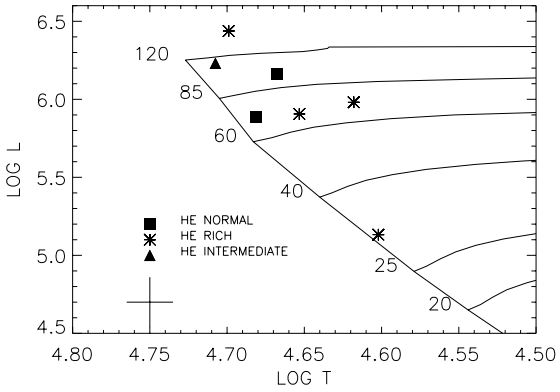

Fig. 7. The programme stars on the Hertzsprung–Russell diagram after the plane–parallel analysis. The meanings of the symbols are those indicated in the lower left corner, together with typical error bars. The theoretical tracks are from Schaller et al. (1992). The numbers to the left of the zero-age main sequence indicate the initial stellar masses in units of solar masses. L is in solar units.

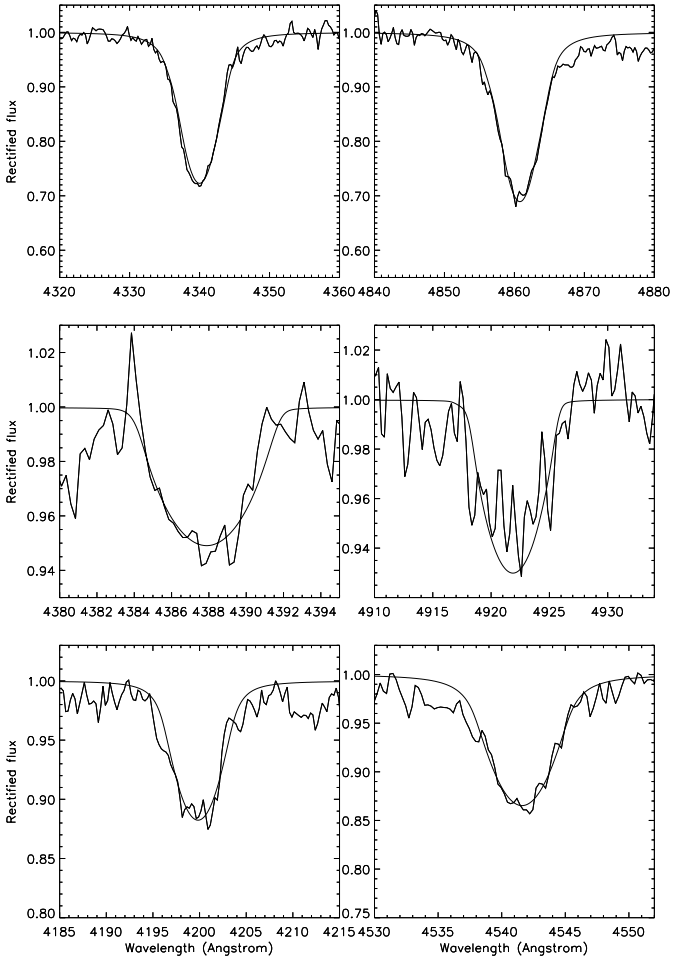

Fig. 8. The fit to the spectral lines in HD 5 689 using the plane–parallel, hydrostatic models, with the parameters given in Table 2. From top to bottom and left to right: H_γ, H_β, He I $\lambda\lambda$4387, 4922, He II $\lambda\lambda$4200, 4541.

4.1. HD 5 689, O6 V

This is the only star for which we can clearly see lines of He I other than He I λ4471. Its line fit, shown in Fig. 8, is obtained at $T_{\rm eff}$= 40 000 K, $\log g$= 3.40, ϵ= 0.25 and $V_{\rm r} \sin i$= 250 km s^{-1}. The rotational velocity, however, is uncertain, as in this cases we only have the He lines (especially He I). The given value can be seen as an upper limit to the projected rotational velocity. We must correct for centrifugal force by adding the term $(V_{\rm r} \sin i)^2/R$, since the measured value is the effective gravity reduced by the centrifugal acceleration, which has to be added here in order to derive the masses. Corrected for centrifugal forces the gravity in Table 2 is $\log g$ = 3.57. As usual for fast rotators, the helium abundance obtained is very large. The radius, however, is very small, and the derived spectroscopic mass is much lower than the predicted evolutionary one. These facts reflect certain problems in the set of parameters for this star. The star has been classified as O6 V by Garmany & Vacca (1991). This classification is not in complete agreement with the star belonging to Cas OB7 (see Humphreys 1978, or Garmany & Stencel 1992), since the absolute magnitude derived from the association distance corresponds to a less luminous object than an O6 V star by one magnitude, which causes the small radius derived (see Table 5 of Vacca et al. 1996). The situation is of course much worse if, based on the low gravity, we associate this star with a giant and adopt parameters characteristics of a luminosity class III object. Thus we have two possibilities: 1) the star is a main sequence star that belongs to Cas OB7, with a smaller radius than usual for its spectral classification, in spite of the large rotational velocity; in this case, the low gravity is difficult to explain, or the models are giving us completely wrong parameters for this star; or 2) the star has parameters typical for a luminosity class III object. In this case, the star would probably not belong to Cas OB7, although we have found no indications in the literature about this possibility. Other combinations of the above arguments are also possible, but the question that something is non-standard with the star remains. This case is very similar to the one we had in Paper I for HD 24 912, which is a known runaway star. Using the Oort constants given by Lang (1980), we obtain a peculiar velocity of 39 km s^{-1} for HD 5689, which, given our uncertainties, does not allow us to decide clearly whether it is a runaway or not, if we adopt the conventional limit of 30 km s^{-1} for runaway stars.

4.2. HD 210 839, O6 I(n)fp

This is λ Cep, a well known fast rotator. The line fit (see Fig. 9) is obtained at $T_{\rm eff}$ = 41 500, $\log g$ = 3.40, ϵ = 0.25 and $V_{\rm r} \sin i$= 250 km s^{-1}. The rotational velocity is again uncertain and could be lower, as we suggest later. This is also indicated by the values found by Penny (1996; 214 km s^{-1}) and Howarth et al. (1997; 219 km s^{-1}). With the centrifugal force correction, $\log g$ increases to 3.47 (see Table 2). The line fit is the best agreement we could find between all the He lines. The parameters are very similar to those of HD 5 689, (except that now the mass discrepancy is only the usual factor 2) but the spectrum shows important differences. λ Cep displays Of features, and

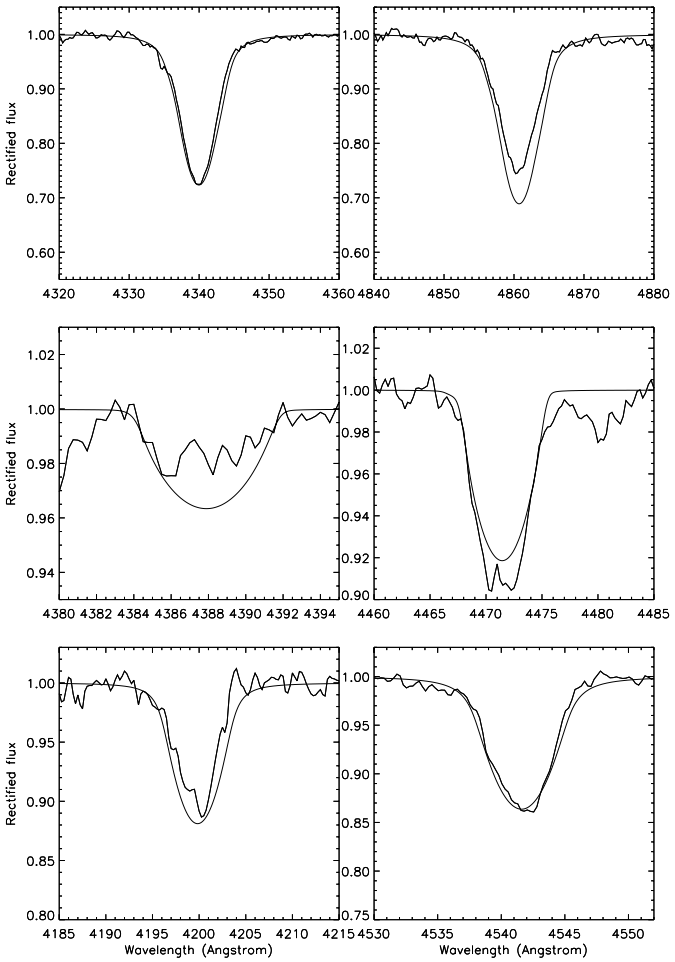

Fig. 9. As Fig. 8, for HD 210 839. Here we show He I λ 4471 instead of He I λ 4922.

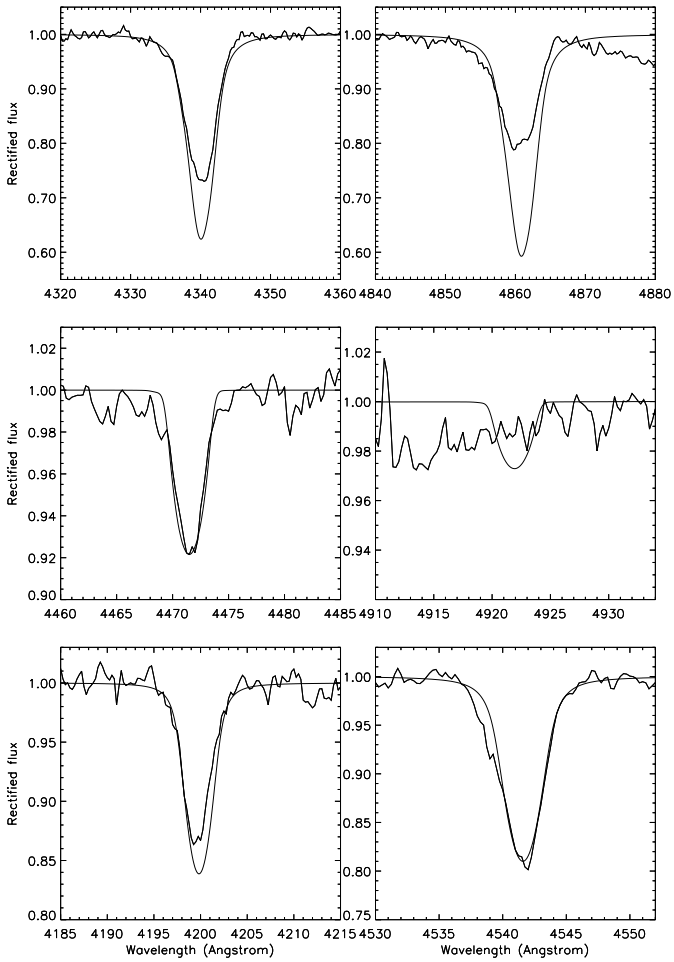

Fig. 10. As Fig. 8, for HD 14 947. Here we show He I λ 4471 instead of He I λ 4387.

has strong emission in H_α. This has to be attributed to the large difference in luminosity (see Fig. 7 and Table 2). In Fig. 7, HD 210 839 occupies the position of an evolved luminous star, already within the instability strip predicted by Kiriakidis et al. (1993). In agreement with this location, λ Cep is known to show profile variations due to non-radial pulsations, which however are below the accuracy of our optical spectra (cf. Fullerton et al. 1996, de Jong et al. 1999). (Note, that we have seen temporal variations in the H_α profile which was observed several times. In contrast, however, two spectra taken in the region from 4200 to 4600 Å showed no significant variations in the lines used for the spectral analysis.) Finally, let us remark that the IR spectrum of λ Cep has been analysed recently by Najarro et al. (1998), who obtained parameters very similar to ours (except in the temperature, for which they find a value lower by 4 000 K, see discussion).

4.3. HD 14 947, O5 If$^+$

The spectral lines of this star are fitted at $T_{\rm eff}$ = 45 000 K, $\log g$ = 3.50, ϵ = 0.15 and $V_{\rm r} \sin i$ = 140 km s^{-1}, which agrees with the value of 133 km s^{-1} given by Penny (1996) and Howarth et al. (1997). The spectral line fits are shown in Fig. 10. The star is an extreme Of (without being a transition object, see Conti et al. 1995), with a large emission in N III λ4630–40 and He II λ4686, and also in H_α. We can also begin to see Si IV λ4116 in emission and the N V $\lambda\lambda$4604, 4620 lines in absorption. The line fit, shown in Fig. 10, can be considered as acceptable. The fit of the He I λ4922 line indicates that the predicted line is a little too strong as compared to the observations, but the difference is very small compared to variations of the line within the error box. The He abundance is not as large as for the two previous objects, but is still larger than solar. The spectroscopic mass is more than a factor of two smaller than the evolutionary one.

4.4. HD 15 558, O5 III(f)

This star is a binary, but we expect the spectrum not to be contaminated, as it is a single component in a well separated system (Mason et al. 1998). The best line fit, shown in Fig. 11, is obtained at $T_{\rm eff}$ = 46 500 K, $\log g$ = 3.70, ϵ = 0.07 and $V_{\rm r} \sin i$ = 120 km s^{-1}. The rotational velocity value agrees with the 123 km s^{-1} of Howarth et al. (1997) although it departs slightly from the one given by Penny (1996) of 147 km s^{-1}. The Of

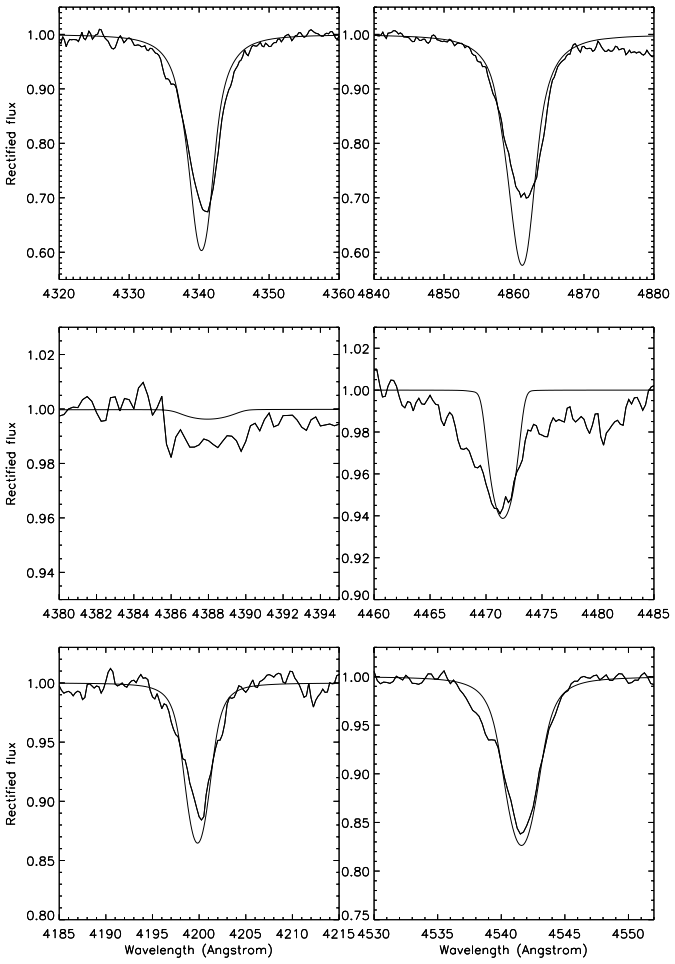

Fig. 11. As Fig. 9, for HD 15 558.

features are weaker than in the previous star, as is the emission in Si IV λ4116, but note that the gravity is now larger. The line fit with hydrostatic models is very difficult. Only the wings of H_γ and H_β are fitted, together with He II λ4541. The singlet He I lines are again too weak and noisy, but in this case also He I λ4471 cannot be fitted. We cannot simply attribute the distortion in the blue wing of He I λ4471 to binarity. If this were the case, we should see the singlet lines too (if the companion is relatively cool) or distortions in the He II lines (if the companion is relatively hot). The lack of a good fit in any He I line makes the parameter determination much less accurate. From the plane–parallel hydrostatic models this is the most massive star, and in fact the mass discrepancy is comparatively low, the difference between the spectroscopic and evolutionary masses being only 30%.

4.5. HD 15 629, O5 V((f))

The best line fit for this star is obtained at $T_{\rm eff}$ = 48 000 K, $\log g$ = 3.80, ϵ = 0.09, with $V_{\rm r} \sin i$ = 90 km s^{-1}. This last value agrees within $\pm$1 km s^{-1} with the values quoted by Penny (1996) and Howarth et al. (1997). In spite of the high temperature, the larger gravity allows us the calculation of hydrostatic models. The line fit is shown in Fig. 12. We can see that the fit is good for the wings of H_γ and H_β, and for He I λ4471 and He II λ4541, but it is bad for He I λ4387, and also for He I λ4922, that is not shown in Fig. 12. We have given much less weight to these two lines, however, because they are very weak and noisy. In the case of He I λ4922, the local continuum has also been placed too low. Correction of this would bring the calculated line into agreement with the observations. More worrying is the lack of fit in the He II λ4200 line. The fit of this line is bad, and comparable to that of the He II λ4686 line, for which we expect a bad fit with hydrostatic models. For this reason we preferred to give more weight to the fit of He II λ4541 than to He IIλ4200. In spite of the large gravity and the luminosity class V, this star also shows the mass discrepancy, which was not the case for less luminous stars in Paper I, where we found no significant mass discrepancy for stars of high gravities. This indicates the increasing role of radiation pressure.

It is interesting to note the case of HD 15 629, HD 14 947 and HD 210 839. Within our error bars, these stars could represent different evolutionary stages of a star of initially around 70 $M_\odot$ following standard evolutionary tracks with mass loss but without rotation. Within this scenario, it is impossible to explain the higher He abundances of the two cooler stars. This can be an indication that rotation plays a strong role in stellar evolution, since there is no other known mechanism that might substantially modify the atmospheric He content of a single star like HD 15 629 in only two Myr. (Another possible scenario for an increased He abundance, close binary interaction, can most probably be discarded in the case of these three particular objects, see Mason et al. 1998). Turning the argument around, if rotation does not play a significant role in the evolution of single massive stars, HD 15 629 could become rather similar to first HD 14 947 and then HD 210 839 in one to two Myr. Unfortunately, we cannot wait to confirm this hypothesis.

4.6. HD 15 570, O4 If$^+$

This star is hotter than the former one, and its Of signatures are stronger (again, without being a transition object, see Conti et al. 1995), indicating a lower gravity. This is confirmed by inspection of the Balmer series, especially the H_α profile, which is strong in emission. From 4600 to 4750 Å we see a broad emission feature with emission lines typical of Of stars, and both Si IV lines neighbouring H_δ are in emission, indicating a large luminosity, which is confirmed. There is also absorption in N V $\lambda\lambda$4604, 4620. It is by far the most luminous star in the sample, and we were not able to fit the spectrum properly for this object. The extreme character of the features allows only a crude guess of the stellar parameters, and we do not show any line fit. Apart from the projected rotational velocity of 105 km s^{-1}, we can only say that the temperature is close to 50 000 K and the gravity should be of the order of $\log g \sim 3.50$ or even less. With the given luminosity, the evolutionary mass is very large, indicating an initial mass in excess of 140 $M_\odot$, which would make HD 15 570 one of the most massive and luminous stars known in the Milky Way. The spectroscopic mass is much

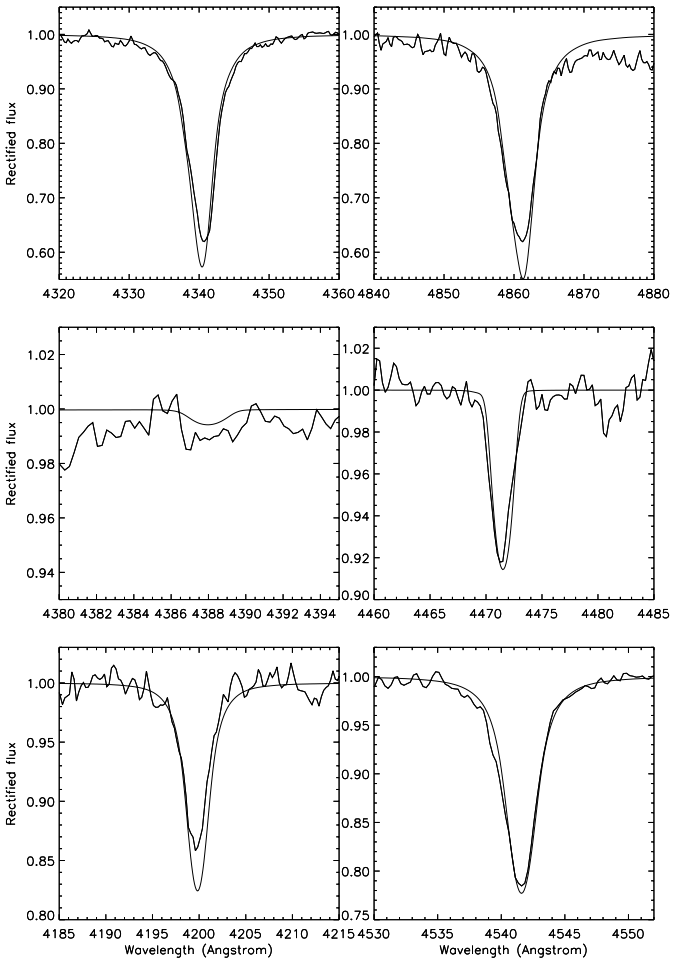

Fig. 12. As Fig. 9, for HD 15 629.

lower, although we have to consider that the gravity has only been "guessed" so far (see next section). There is a chance that the star is helium enhanced, and we adopt ϵ = 0.15.

*4.7. Cyg OB2 #7, O3 If**

This is a very hot star. He I λ4471 is only marginally seen, and the emission in N IV λ4058 and the absorptions in N V $\lambda\lambda$4604, 4620 are strong. We again find the broad emission feature with emission lines typical for Of stars, and both Si IV lines neighbouring H_δ in emission. In spite of our efforts, we were unable to fit the star with plane–parallel models, the required gravities being too low. As for HD 15 570, we had to extrapolate the plane–parallel parameters, and we do not show a line fit. The final parameters we adopt are $T_{\rm eff}$ = 51 000 K, $\log g$ = 3.65, ϵ = 0.12 and $V_{\rm r} \sin i$ = 105 km s^{-1}. We did not succeed in calculating models in this range ($\log g$ had to be larger at least by 0.1), and spherical models including mass-loss are obviously required. This star is also very luminous and massive, with an initial mass in excess of 110 $M_\odot$, but with a large mass discrepancy.

5. Analysis with spherical models with mass-loss

The difficulties in the analysis of some of the spectra discussed in the previous section result from the neglect of sphericity and mass-loss effects. Thus, we decided to use the program described by Santolaya–Rey et al. (1997) to account for these effects. Briefly, this program constructs a unified model of the stellar photosphere and wind regions, with a number of standard (stationarity, homogeneity) and non-standard assumptions and approximations (the most important of the latter concerns the way the temperature structure is obtained, which results in well approximated, but not forced, flux conservation throughout the atmosphere and a constant temperature in the wind). It solves the line-formation problem in an expanding atmosphere with spherical geometry, and Stark broadening is included in the final formal solution.

The atomic models used are the H and He models used also in our plane–parallel analysis, with minor changes to adapt them to the new program. Line-blocking has not been included so far. Its influence, however, will be considered in the next section (at least on a qualitative basis), and has affected the results decribed here.

We have adopted the following procedure. We begin with the parameters given by the plane–parallel models (see Table 2). The values of the terminal velocities are taken from Puls et al. (1996), except for HD 15 570 (from Lamers & Leitherer 1993) and for Cyg OB 2 #7 and HD 5689, where we have adopted the V_∞ – spectral classification relation provided by Haser (1995). The last object has been assigned a V_∞ corresponding to an O6 III star, which is a compromise between the luminosity class V given by Garmany & Stencel (1992) and the low gravity obtained from our analysis (see the discussion in the preceding section). Note, that this compromise is reasonable, since the difference between the mean V_∞ of O6V and O6I stars is only 450 km s^{-1}.

Also needed are the values of the β exponent in the β–velocity law. For HD 15 558, HD 15 629 and HD 210 839 we adopted the values given by Puls et al. (1996). For HD 14 947, also analysed by Puls et al., we adopted β = 1.15 instead of 1.0 as quoted by Puls et al., for reasons explained later in the discussion of HD 14 947. For Cyg OB2 #7, HD 15 570 and HD 5 689 which were not analysed by Puls et al we used β= 0.8, 1.0 and 1.0, respectively.

For each star we have constructed a small model grid by varying gravity, temperature and mass–loss rate. We then tried to fit H_γ, H_α and the ratio He II λ4200 to He I λ4471, which is our new preferred temperature indicator, following the results described in the next section, where we will show that this He II line is less sensitive to model details than He II λ4541. Of course, the use of a new temperature indicator introduces also an additional difference to the results from our plane–parallel considerations.

All other parameters remain fixed at the beginning at their values determined from the plane–parallel analysis. When necessary, the helium abundance has been changed later. The radius merits additional comments. Its value is derived from the emer-

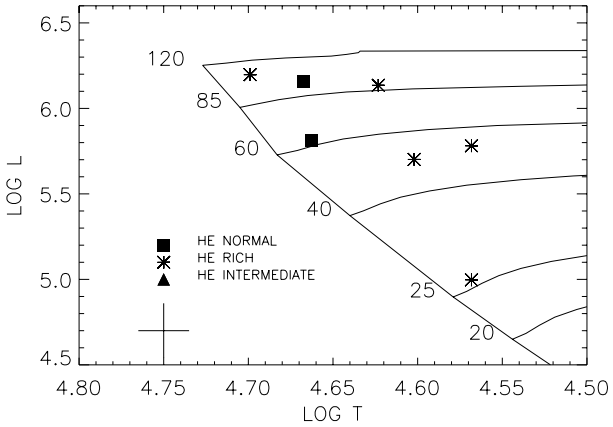

Fig. 13. The programme stars on the Hertzsprung–Russell diagram after our analysis with spherical models with mass-loss. Compare the new diagram with Fig. 7. Details are as in Fig. 7.

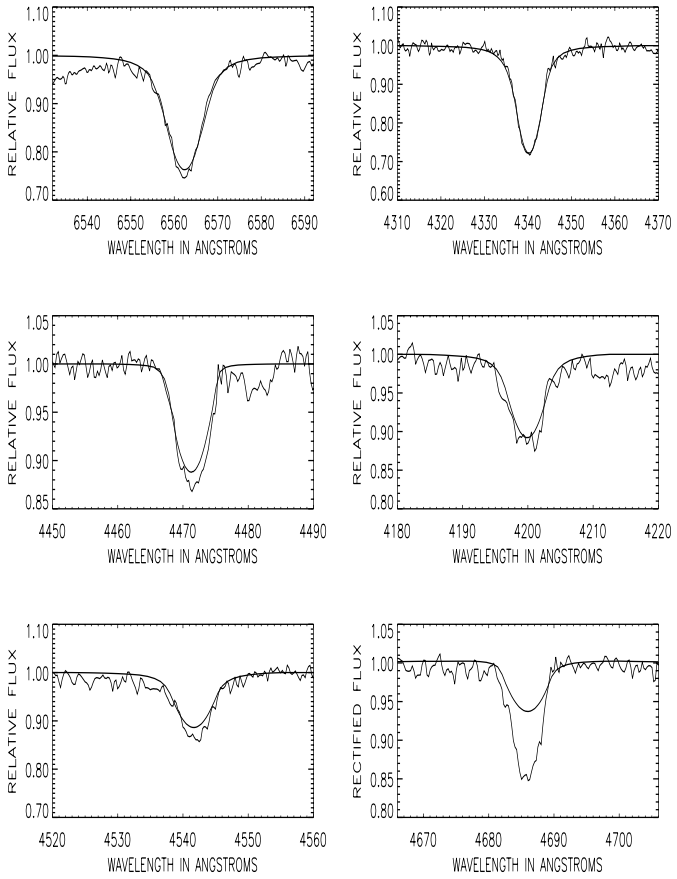

Fig. 14. Fit to the H and He lines in HD 5 689 using a spherical model with the parameters given in Table 3. From left to right and top to bottom we show H_γ, H_α, He I 4471, He II 4200, He II 4541 and He II 4686. Wavelengths (along the abscissa) are given in Å. The ordinates give the relative fluxes.

gent flux, which has been obtained for a given set of parameters (those from the plane–parallel analysis). Changing the parameters will change the derived radii, and thus an iteration process might be required. We have recalculated the radii of our objects with the new parameters, and have obtained an average change of only 2% (the maximum change being of only 4.5%, from 22 to 23 $R_\odot$). Thus we used the plane–parallel values without further iteration. The finally adopted and derived parameters are summarized in Table 3. For those stars which have been analysed by Puls et al. (1996), we give their results in Table 4 for comparison. The new position of the stars in the HR diagram is shown in Fig. 13.

5.1. HD 5 689, O6 V

We can see the line fit to this star in Fig. 14, for a model with $T_{\rm eff}$ = 37 000 K, $\log g$ = 3.45 (which increases up to 3.57 due to the centrifugal correction) and log $\dot{M}$ = –6.80. The temperature is lower than in the plane–parallel case, in part due to the change of our temperature criterion. The gravity, however, remains the same (which actually implies an increase with respect to plane–parallel models, since a lower temperature usually demands a lower gravity to fit a given line). Thus, the large mass discrepancy found above (see Table 2) cannot be reduced by the spherical models, since it originates from the low value of the radius, rather than from the low gravity. Neither can we decide whether the star has a larger radius in parallel with a higher mass–loss rate, since the H_α wind-emission depends only on the ratio ($\dot{M}$ /$R^{3/2}$), whereas its photospheric component is independent of both. Assuming an absolute magnitude of a typical O6 III star (M_V = –5.78 mag, see Table 6 of Vacca et al. 1996) results in a radius of 15.9 $R_\odot$, but does not change the fit quality (it affects only slightly the fit of He I λ4471). Of course, mass, luminosity and mass-loss rate would be affected and we would obtain a spectroscopic mass of 30.0 $M_\odot$, an evolutionary mass of 41.9 $M_\odot$ (thus reducing the mass discrepancy to 30%, a typical value), a luminosity of 5.6, closer to the other objects (see also the discussion in Sect. 7) and a logarithmic mass-loss rate of -6.17. However, this possibility would also imply that the wind in HD 5689 is much less efficient than in HD 210 839, as both stars would have roughly similar parameters, except for $\dot{M}$. Unfortunately, without knowing the distance to HD 5689 more accurately, we cannot derive stronger conclusions. We also see that He II λ4541 does not fit completely, and in particular the fit of He II λ4686 is poor. This line always shows a poor fit, with an observed absorption that is much stronger than predicted, especially in the blue wing. As explained in the following section, this seems to be related to lack of line-blocking in our models, and He II λ4541 seems also to be affected, although to a lesser extent.

5.2. HD 210 839, O6 I(n)fp

The line fit of this star, shown in Fig. 15, reveals two problems. First, the form of H_γ suggest that the adopted rotational velocity is too large. A value of 200 km s^{-1} results in a much better fit[2]

[2] a misprint in Table 8 of Puls et al. (1996) gives a velocity of 100 km s^{-1} for this star, whereas 200 km s^{-1} was the value adopted in that work. and would agree with previous determinations (Conti & Ebbets

Table 3. Parameters determined for the programme stars starting with the parameters from Table 2 and using the spherical models with mass-loss. Temperatures are in thousands of Kelvin, velocities in km s^{-1} and mass-losses in solar masses per year. MWM stands for modified wind momentum, and given is log ($\dot{M}\,V_\infty R^{0.5}$), with $\dot{M}$ in solar masses per year, V_∞ in km s^{-1} and R in solar radii. $M_{\rm s}$, $M_{\rm ev}$ and M_0 are, respectively, the present spectroscopic and evolutionary masses, and the initial evolutionary mass, in solar units. The last column indicates whether we formally have a mass discrepancy considering an error of 0.22 in log($M_{\rm s}$).

Star	$T_{\rm eff}$	$\log g$	ϵ	$R/R_\odot$	$\log(L/L_\odot)$	V_∞	β	log $\dot{M}$	$M_{\rm s}$	$M_{\rm ev}$	M_0	MWM	M discr.?
Cyg OB2 #7	50.0	3.72	0.18	16.7	6.20	2900	0.80	–4.95	53.0	104.5	107	29.93	Yes
HD 15 570	42.0	3.80	0.15	22.0	6.14	2600	1.05	–4.75	112.6	79.6	89	30.14	No
HD 15 629	46.0	3.81	0.09	12.7	5.81	3000	1.00	–6.13	37.5	61.4	63	28.70	No
HD 15 558	46.5	3.86	0.07	18.5	6.16	2800	0.75	–5.40	89.5	91.7	97	29.48	No
HD 14 947	40.0	3.67	0.20	14.8	5.70	2400	1.15	–5.25	36.8	47.5	49	29.52	No
HD 210 839	37.0	3.55	0.25	18.9	5.78	2250	0.90	–5.17	45.8	49.3	52	29.62	No
HD 5 689	37.0	3.57	0.25	7.7	5.00	2500	1.00	–6.80	7.9	25.4	26	27.85	Yes

Table 4. Parameters as determined by Puls et al. (1996) for some of the stars in Table 3. Units are as in Table 3.

Star	$T_{\rm eff}$	$\log g$	ϵ	$R/R_\odot$	$\log(L/L_\odot)$	V_∞	β	log $\dot{M}$	log ($\dot{M}\,V_\infty R^{0.5}$)
HD 15 629	47.0	3.90	0.07	14.2	5.95	3000	1.00	–6.12	28.73
HD 15 558	48.0	3.85	0.07	21.8	6.36	2800	0.75	–5.14	29.78
HD 14 947	43.5	3.50	0.15	16.1	5.93	2350	1.00	–5.12	29.65
HD 210 839	38.0	3.65	0.09	19.0	5.83	2250	0.90	–5.28	29.52

The second problem is that we were unable to fit the P Cygni form of the H_α–profile. As was pointed out previously, λ Cep is a possible non-radial pulsator (Fullerton et al. 1996, de Jong et al. 1999), which might induce deviations from homogeneity (by exciting the line-driven wind instability already in the lower wind part, see Feldmeier et al. 1997), and the large rotation rate might have an additional influence on the wind structure and the resulting profile (cf. Owocki et al. 1998 and references therein; Petrenz & Puls 1996). We decided to concentrate on the red wing of H_α, since the theoretical simulations result in a blue wing affected by an extra He II absorption, which is inadequately described in our present models (see next section), and any wind variability becomes much more visible in the blue wing, compared to the red one. Again, the predicted emission in He II λ4686 is much stronger than observed; also, the temperature is lower than in the plane–parallel case. However, the gravity is larger, and we do not find a mass discrepancy for this star.

λ Cep has been also analysed by Puls et al. (1996), who adopted slightly different parameters. The main difference is the helium abundance (ϵ = 0.09 instead of 0.25), which has a small influence on the gravity, however produces a larger wind momentum with a lower luminosity in our present results. (The value for ϵ quoted by Puls et al. was not derived from a consistent spectral analysis, however taken from the literature). It is interesting to note that the high abundance favoured by our findings is in agreement with Blaauw's suggestion that all runaway stars are He enriched (Blaauw 1993). Note also that the possible runaway nature of HD 5 689 fits within this scenario.

Finally, we point out that our mass–loss rate coincides well with other determinations from H_α by Lamers & Leitherer (1993), but is larger than that derived from radio fluxes (Lamers & Leitherer 1993) by a factor of 3.

5.3. HD 14 947, O5 If$^+$

The analysis of HD 14 947 has been hindered by an inconsistency in the radial velocities derived from the blue and the red spectrum (the spectra were taken in September 1991 and August 1992, see Table 1). While in the blue spectrum there are several metal lines to derive the radial velocity correction, in the red spectrum we only have three lines of He II and they give a result that is incompatible with that of the blue metal lines. Mason et al. (1998) list this star as having a constant radial velocity and thus we don't have a clear explanation for the radial velocity change. Therefore, the radial velocity correction for this star is particularly inaccurate. We have adopted the correction indicated by the blue metal lines, accounting for the different rest frames as a function of observation date.

The line fit of H_γ is comparatively poor for this star (see Fig. 16). This reflects a problem that we have found for the first time, an inconsistency between the fit for H_γ and H_α. The fit for H_γ would need a mass-loss rate which is only half that of H_α. This inconsistency is only weakly dependent on the gravity.

The new temperature derived for HD 14 947 is much lower than that obtained from plane–parallel models. This is due

1977, Penny 1996, Howarth et al. 1997). A change in the rotational velocity would not change the adopted parameters, only the quality of the line fit. We show the fit with the value adopted for the plane–parallel analysis, although a better fit is possible with the lower $V_{\rm r} \sin i$ value.

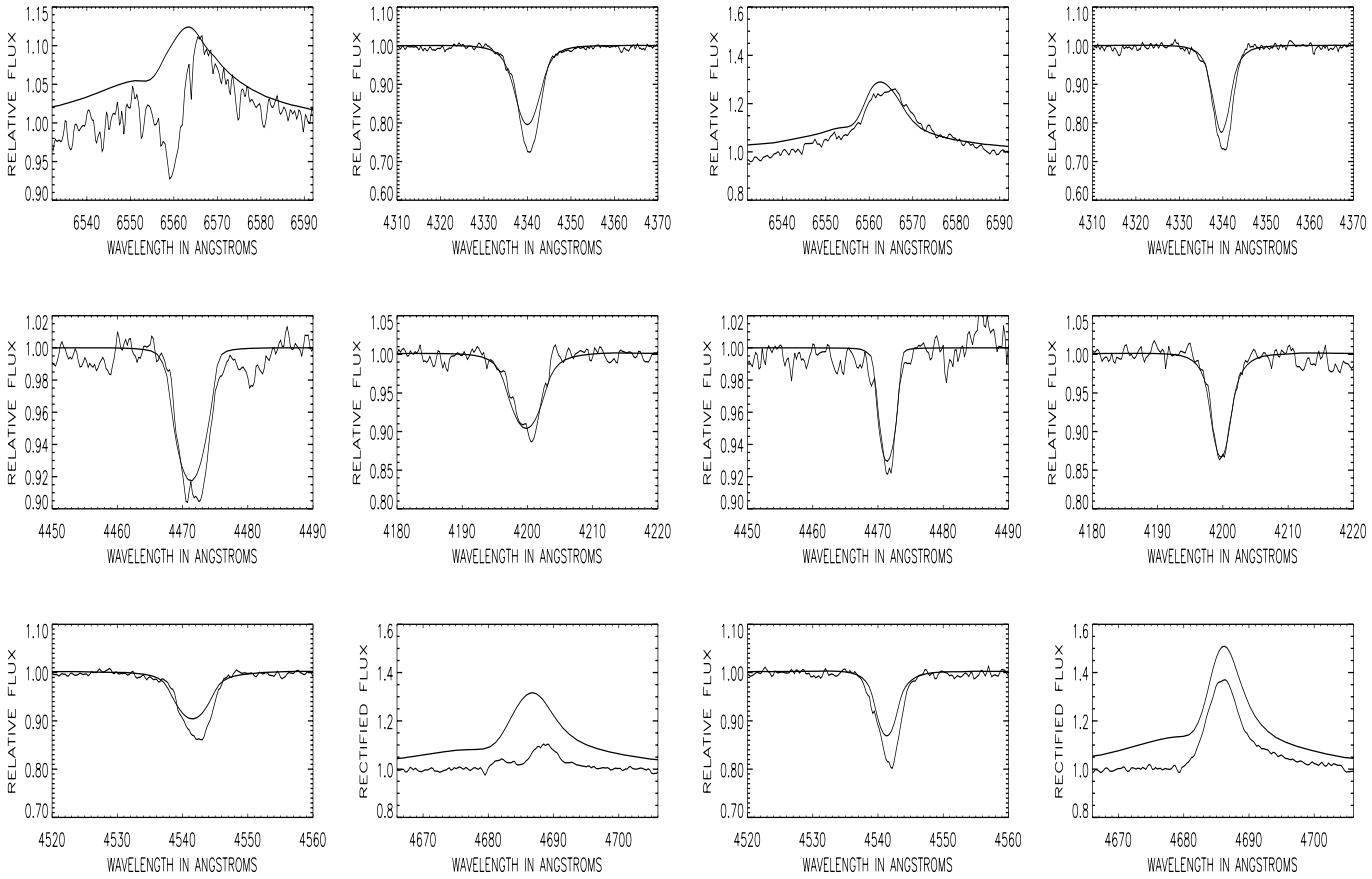

Fig. 15. As Fig. 14, but for HD 210 839. The fit of H_γ improves considerably if the adopted rotational velocity is lowered from 250 to 200 km s^{-1}.

Fig. 16. The line fit to HD 14 947 using spherical models with mass-loss. We see the comparatively poor fit for H_γ in the core, which can be largely improved by reducing the mass–loss rate by a factor of two.

to sphericity together with the new criterion of using He II λ 4200. Again, in agreement with the large mass–loss rate, He II $\lambda\lambda$4541, 4686 are poorly fitted, (see discussion in the next section).

The spectroscopic mass derived is clearly lower than the evolutionary one, although they agree within the errors. The analysis by Puls et al. (1996) gave slightly different stellar parameters, the most important difference being the now lower temperature implying a lower luminosity by 0.23 dex.

There is an upper limit of $10^{-4.75}$ $M_\odot$/yr for the mass–loss rate of HD 14 947 derived from radio fluxes (Lamers & Leitherer 1993). The value we find here is in agreement with this upper limit.

5.4. HD 15 558, O5 III(f)

The line fit to HD 15 558 obtained for the parameters given in Table 3 can be seen in Fig. 17. The mass–loss rate is rather large, in agreement with the high luminosity, especially when compared with HD 15 629, a star that could be considered similar at first inspection since both H_α profiles are in absorption. However, the value we obtain here for $\dot{M}$ is lower than that obtained by Puls et al. (1996) due to the change in the stellar parameters. The gravity is largely increased with respect to the value derived with plane–parallel, hydrostatic models (by 0.15 dex), and in fact the derived spectroscopic mass is nearly equal to the evolutionary one, thus making HD 15 558 one of the few cases for which we do not find any mass discrepancy. The generally good agreement in the line fit to HD 15 558 is again broken by He II λ4686.

5.5. HD 15 629, O5 V((f))

The line fit of HD 15 629 is obtained for the parameters given in Table 3 and is shown in Fig. 18. We see that the mass–loss rate is relatively low and agrees very well with the value given by Puls et al. (1996). The gravity we obtain is similar to that in the plane–parallel case, and thus the new mass is again lower than the evolutionary one, although there is formal agreement considering the error bars. The worst fit corresponds to He II λ4686. A comparison with Puls et al. (1996) shows that both sets of values are compatible, although the general trends (lower temperatures, radii and luminosities in our case) remain.

5.6. HD 15 570, O4 If$^+$

This is an extreme object, and the adopted parameters are actually a compromise, reflected in very large uncertainties. For this

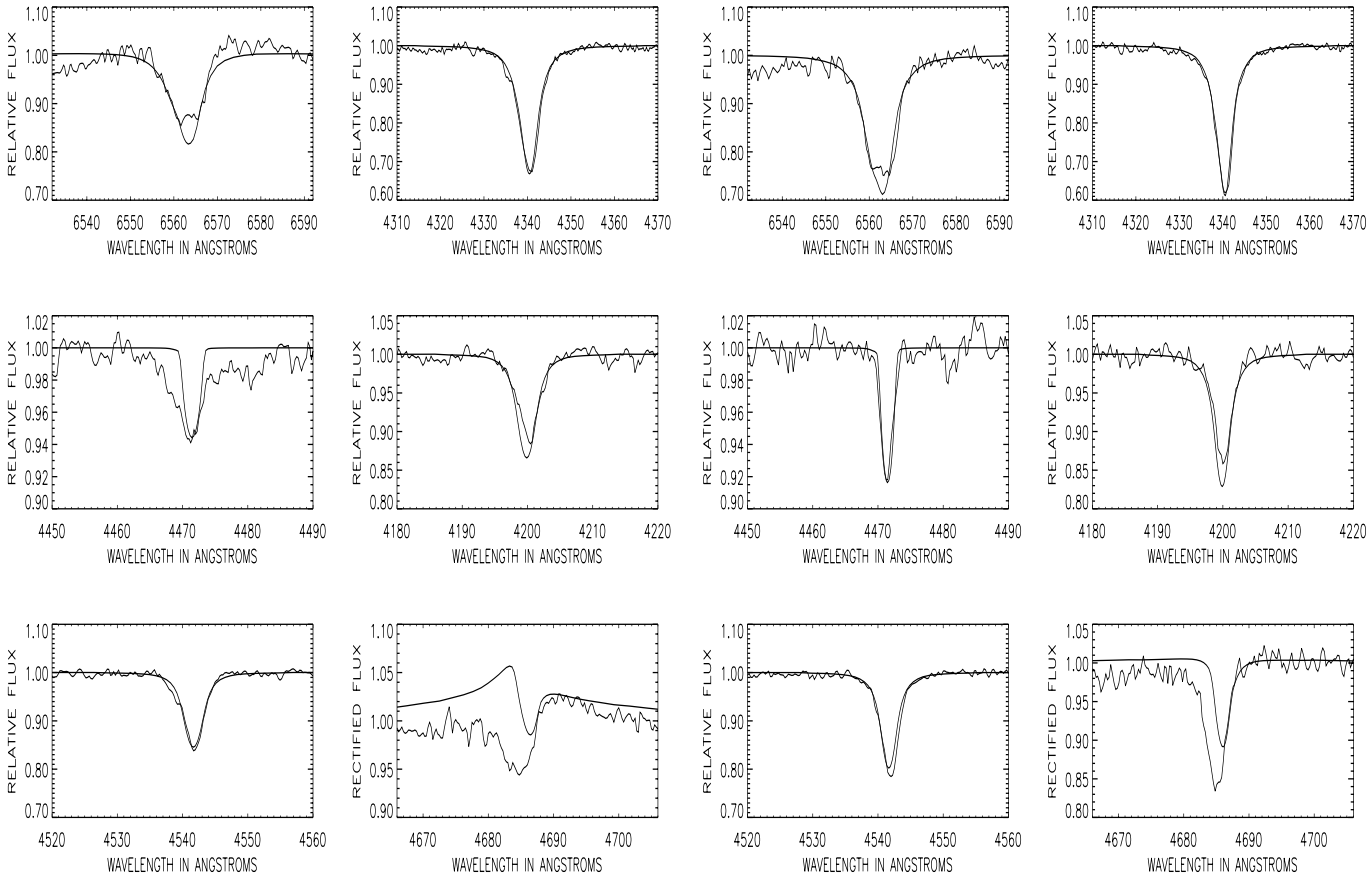

Fig. 17. As Fig. 14, but now showing the line fit to HD 15 558.

Fig. 18. As Fig. 14, for HD 15 629.

star we derive $T_{\rm eff}$ = 42 000 K, $\log g$ = 3.80, ϵ = 0.15, log $\dot{M}$ = -4.75 (see Table 3 for the rest of the parameters). The very high mass–loss rate results in an extreme insensitivity of the wings of H_γ to gravity variations, as can be seen in Fig. 19, where we have plotted the profiles for $\log g$ = 4.05 and $\log g$ = 3.55. These can be considered as limits beyond which the fits begin to become poorer than for the range [3.55,4.05]. Thus we have adopted $\log g = 3.80 \pm 0.25$. However, it should be borne in mind that even such a large error is optimistic, as the uncertainty of the radial velocity correction has not been included. Also the He profiles are largely insensitive to $\log g$ variations, but they allow us to restrict $T_{\rm eff}$ and ϵ.

The line fit to this star is shown in Fig. 20. A detailed fit of the strong H_α emission of HD 15 570 was not possible, since for the given parameters the simulations always showed a double peak due to the extra emission coming from the He II blend (see the discussion in the following section) not seen in the observations. Thus the adopted criterion was to fit the red wing of H_α. Again, we found the same problem encountered for HD 14 947. The best fit of H_γ gives a mass–loss rate different from the best fit of H_α, without any possibility to fit both simultaneously, with a discrepancy of roughly a factor of two. H_α indicates a value of about log $\dot{M}$ = –4.75 and H_γ one around log $\dot{M}$ = –5.0, but this low value of log $\dot{M}$ would also imply that the gravity is lower than in the case of higher mass–loss rate. This is shown

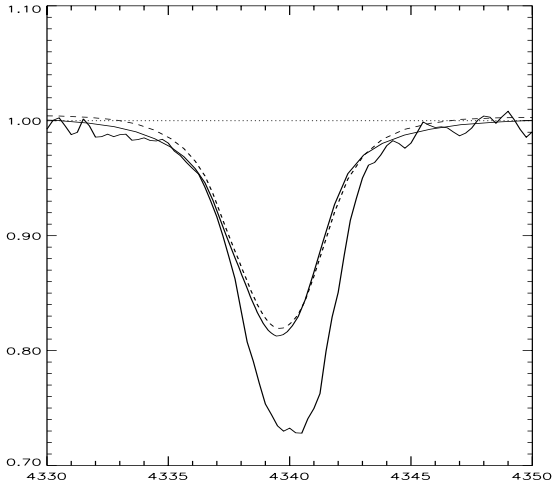

Fig. 19. The line fit to H_γ in HD 15 570 with $\log g$ = 4.05 (solid line) and $\log g$ = 3.55 (dashed line). All other parameters are as in Table 3. The abscissa gives wavelength in Å and the ordinate relative fluxes.

in Fig. 21, where we see the fit for H_γ at log $\dot{M}$ = –4.75 and –5.0 at $\log g$ = 3.80. Comparing with Fig. 19 we see that the effect of lowering the mass–loss rate is larger than any change of gravity at log $\dot{M}$ = –4.75. At the lower log $\dot{M}$ of –5.0 we would obtain a lower and more constrained gravity, but it is impossible to obtain even a moderate fit to H_α. In any case, the mass–loss rate

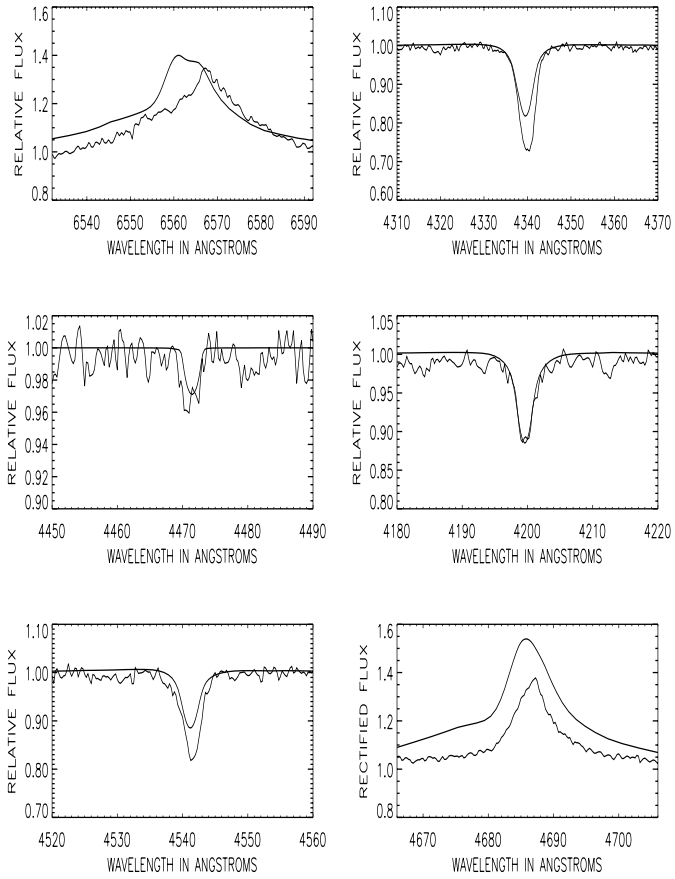

Fig. 20. The line fit for HD 15 570. The fit shown corresponds to the model fitting the red wing of H_α (see text).

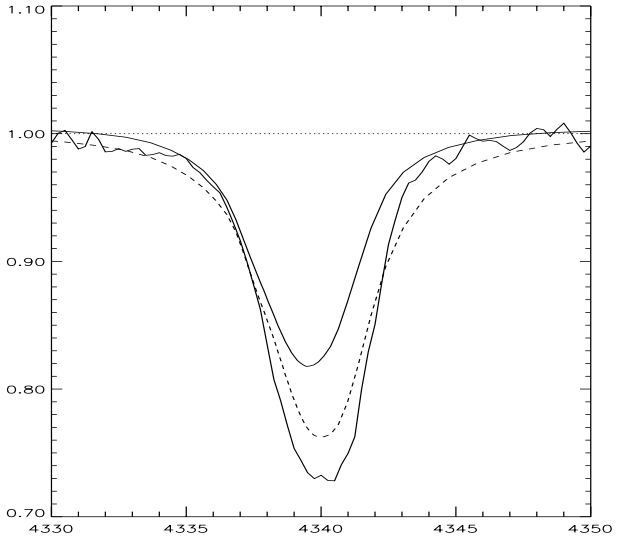

Fig. 21. The line fit to H_γ in HD 15 570 with log $\dot{M}$ = –4.75 (solid line) and log $\dot{M}$ = –5.00 (dashed line) at $\log g$ = 3.80. All other parameters are as in Table 3. Comparing with Fig. 19 we see that for this strong wind, changing the mass–loss rate has a larger effect than changing the gravity. The abscissa gives wavelength in Å and the ordinate relative fluxes.

is very large, although we should point out again that our mass–loss rate coincides well with other H_α determinations (Puls et al. 1996; Lamers & Leitherer 1993) but it is larger than that derived from radio fluxes (Lamers & Leitherer 1993) by a factor of 4 if we adopt the value from the fit of H_α, and by a factor of 2 if we take the one more consistent with H_γ.

The temperature is now much lower than in the plane–parallel case, as for HD 14 947, again due to the combined effects of sphericity and the new criterion for the He ionization equilibrium. In agreement with this, the fit to He II $\lambda\lambda$4541, 4686 is poor. The formal change in $\log g$ is large with respect to the plane–parallel values (0.20 dex) and now HD 15 570 has also the largest spectroscopic mass, even formally exceeding 100 $M_\odot$. Little can be said about the actual mass and the mass discrepancy. In Table 3 we see that the spectroscopic mass is 30% larger than the evolutionary one, but we did not attemp to bring both into agreement (which could be possible adopting $\log g$ = 3.65), since for HD 15 570 gravity and mass are only formal values in the centre of a large uncertainty area, and have to be regarded as rather inaccurate. It is clear however that HD 15 570 is one of the most extreme O stars in the Milky Way, and probably one of the most massive stars.

*5.7. Cyg OB2 #7, O3 If**

The line fit for this star, displayed in Fig. 22, shows similar problems to those of HD 14 947 and HD 15 570 discussed before. The mass–loss rate is quite large, again exceeding 10^{-5} $M_\odot$/yr, and the parameters point to a very massive star. The large mass–loss rate results in a change of $\log g$ with respect to the plane–parallel hydrostatic models, which is relatively large (0.15). However, the mass discrepancy is still present, since the spectroscopic mass is still a factor of 2 lower than the derived evolutionary mass. Another important change with respect to plane–parallel models is the new helium abundance, now ϵ= 0.18. It is interesting to note that Herrero et al. (1999) could not find evidence of any helium discrepancy in their analyses of other, less extreme Cyg OB2 stars.

6. Additional considerations

6.1. The H_γ problem

As we have seen in the foregoing analysis, for three of our objects with dense winds the wind emission seen in H_γ is inconsistent with the mass–loss rate derived from H_α. It may be questioned why this obvious problem has not already been discovered by Puls et al. (1996) who found no such discrepancy and derived— for the object common to both investigations (HD 14 947[3]) —a lower value for $\log g$ than follows from our analysis.

This difference has the following origin. For the problematic objects, the Doppler *core* of H_γ becomes optically thick in the

[3] Note, that HD 15 570 has not been analysed by Puls et al. by means of detailed profile fits. Instead, only previously published values for equivalent widths have been used, so that any comparison is obsolete.

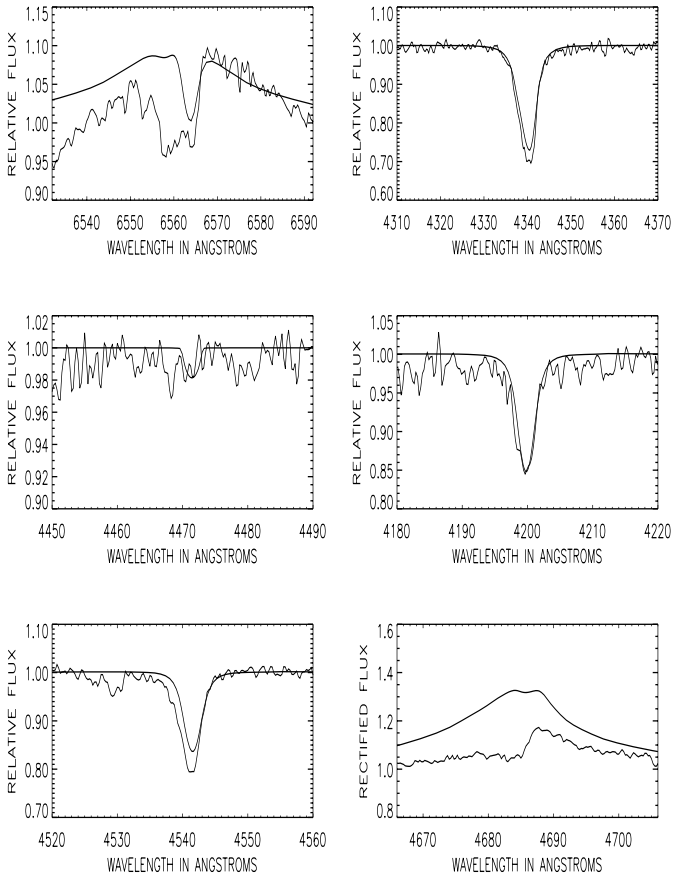

Fig. 22. The line fit for Cyg OB2 #7 using a spherical model with the parameters given in Table 3.

wind. Thus, it depends only on the wind conditions (mainly in the transonic region) and is independent of any underlying photospheric radiation. Consequently, it can be correctly fitted by the approach described in Puls et al. and would compare to our results.

On the other hand, the *wings* of H_γ depend on the illuminating radiation from below the transonic region. In the concept applied by Puls et al., this radiation was taken from photospheric profiles calculated on the basis of *hydrostatic* models, and the wind contamination was correctly accounted for. The fitted $\log g$ value was finally corrected for the difference between hydrodynamic and hydrostatic atmospheres, accounting for the different formation depths in an approximate and *global* way, where the correction turned out to be only moderate in the parameter space considered.

This procedure, however, is only justified if the major part of the wings is actually formed in some pseudo-hydrostatic environment, which is the case if the wind densities are not too high. For increasing wind density, however, the difference between hydrostatic and hydrodynamic stratification (e.g., Puls et al., Fig. 16) becomes increasingly larger, and the point where the transition between both regimes occurs shifts to correspondingly larger (mean) optical depths. Thus, for higher wind densities only the far wings are formed in a purely hydrostatic environment, whereas the inner wings are severely affected by the wind conditions, which display a lower density at given optical depth. Consequently, the use of hydrostatic profiles and the global correction applied by Puls et al. will inevitably fail under those conditions. Moreover, the derived values for $\log g$ will be too small compared to "reality", since, for a given $\log g$, the hydrostatic densities are always larger than those in the wind regime. As a result, the deviations between the profiles calculated by Puls et al. and ours should become largest just outside the Doppler core, and vanish at the extreme wings. Thus, it is not too surprising that the results of our *consistent* description deviate from the results given by Puls et al. with *respect to gravity* (derived from the wings), whereas the H_γ Doppler cores would be consistent with the mass–loss rate derived from H_α, however are unfortunately not visible due to rotational broadening.

We like to point out that for a (small) number of objects with denser winds the determination of the stellar mass becomes completely impossible, since in those cases even the continuum is formed in the wind and the reaction of *any* profile on pressure scale height becomes impossible.

In order to check under which conditions this problem will arise, we have calculated the (minimum) continuum optical depth given by electron scattering as function of wind parameters:

$$\tau_e = \int_r^\infty \rho(r)\mathrm{d}r,\ \approx 0.4\ \mathrm{cm}^2/\mathrm{g}\ \frac{1+I_{\rm He}Y}{1+4Y}, \qquad (1)$$

with $s_{\rm e}$ the electron scattering mass absorption coefficient, Y the helium abundance (by number) with respect to hydrogen and $I_{\rm He}$ the number of free electrons provided per He atom. By means of the equation of continuity and for the β velocity law which is used also in our model simulations,

$$v(r) = v_\infty\big(1-\frac{bR_*}{r}\big)^\beta,\ b = 1-(v_o/v_\infty)^{1/\beta} \qquad (2)$$

(where $v_o \approx 0.1 v_{\rm sound}$ is the velocity at the transition point between pseudo-hydrostatic and wind region, cf Santolaya–Rey et al., 1997, their Sect. 2.2), we have

$$\tau_e(v) = \frac{\dot{M}s_{\rm e}}{4\pi R_* v_\infty}\frac{1}{b\beta}\int_{v/v_\infty}^1 v'^{(\frac{1}{\beta}-2)}\mathrm{d}v', \qquad (3)$$

where $v' = v(\mathrm{r})/v_\infty$. Inserting typical parameters and denoting by A the optical depth-like quantity

$$A = \frac{\dot{M}}{10^{-6}\mathrm{M}_\odot/\mathrm{yr}}\ \frac{10\mathrm{R}_\odot}{R_*}\ \frac{1000\,\mathrm{km/s}}{v_\infty}\ \frac{1+I_{\rm He}Y}{1+4Y}, \qquad (4)$$

the electron scattering optical depth is finally given by

$$\begin{aligned}\tau_e(v)\ &\approx\ 0.028\,A\,(-\ln\frac{v}{v_\infty})\quad \text{for}\ \beta=1\\ &\approx\ 0.028\,\frac{A}{1-\beta}\left(1-(\frac{v}{v_\infty})^{\frac{1-\beta}{\beta}}\right),\ \beta\neq 1\end{aligned} \qquad (5)$$

(approximating b by unity). In Fig. 23 we have plotted this quantity, evaluated at $v/v_\infty = 0.001$ (which compares roughly with the velocity at the transition point for hot stars) as a function of

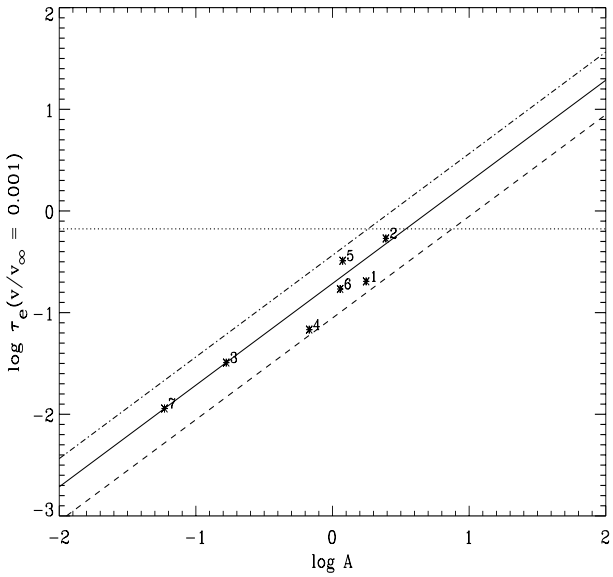

Fig. 23. Electron scattering optical depth at transition velocity $v/v_\infty = 0.001$ as function of A (cf. Eq. (4)) and β = 1.3 (dashed-dotted), 1.0 (fully drawn) and 0.7 (dashed). The positions of our programme stars (according to the derived wind parameters) have been indicated by asterisks.

A and β. The dotted line gives the optical depth of 2/3, and for all objects with $\tau_e(A) > 2/3$ the continuum is definitely formed in the wind. We have indicated the position of our sample stars by asterisks, where the number refers to Table 1. Obviously, object no. 2 (= HD 15 570) lies just at the border line, and thus a gravity determination is almost impossible (cf. Fig. 19 for the influence of gravity on H_γ). For the objects nos. 1 (Cyg OB2 #7), 5 (HD 14 947) and 6 (HD 210 839) at least the inner wings of H_γ are severely affected by the wind, and thus result in a larger gravity than found by Puls et al. 1996 (if all other parameters remain the same). For the remaining three stars, the continuum is formed solely in the hydrostatic part, and the derived numbers should coincide with the approximate method, as is actually the case.

6.2. Influence of He II resonance lines

Those readers in particular who are not well familiarized with spectral analyses of hot stars may question why we did not take the most prominent line of He II in the optical part of the spectrum, namely He II 4686 ($n = 3 \rightarrow 4$), into consideration so far (although we have plotted it for all models and the discrepancy is obvious). This question is completely legitimate, since the upper level of this transition is just the lower one of our strategic lines He II $\lambda\lambda$ 4200, 4541, and should be reproduced with a similar degree of precision if our models were reliable.

However, it is well known that this line (if formed in the wind) is extremely difficult to fit, and, to our knowledge, has never been used in any kind of NLTE-analysis of luminous O-stars. Usually, if one compares the predicted profiles to observations, the synthetic line turns out to be too strong in emission, even if all other lines including H_α do perfectly fit.

This rather unsatisfactory behaviour, which is normally bypassed by simply excluding He II 4686 from the line list, relates to the extreme sensitivity of the participating levels on the treatment of the He II resonance lines and their sensitivity to line-blocking (for a discussion concerning this problem of the formation of He I-lines, cf. Santolaya–Rey et al. 1997; see also the related discussion concerning the ionization structure of WRs by Schmutz 1997). In standard simulations for wind conditions as described here, where line-blocking effects are excluded, the dominating background "opacity" below 303 Å (referring to He II Ly_α) is Thomson *scattering*, leading to extremely enhanced radiation temperatures at the resonance-line' frequencies. Compared, for example, to a detailed balance situation (see below), the ground-state becomes depopulated, which in consequence (and in connection with the increased escape-probabilities due to the velocity field) prohibits He III from recombining and gives rise to much weaker absorption edges at 229 Å, compared to plane–parallel simulations (cf. Gabler et al. 1989, especially Fig. A2).

Moreover, since the radiation temperature is increasing towards higher frequencies (due to the decreasing bf-opacity at lowest photospheric levels), the NLTE departure coefficients are larger for higher levels than for lower ones. Thus, in addition to the wind emission by geometrical effects, the lines between excited levels (predominately He II 4686) are contaminated by a strong source function $\propto b_{\rm upper}/b_{\rm lower} > 1$, which leads to a much stronger total emission than would be the case if the resonance lines were of less importance. Actually, a pilot investigation by Sellmaier (1996) for the case of ζ Pup has shown that the emission of He II 4686 could be significantly reduced if line-blocking was accounted for correctly.

In order to investigate in how far the above effects are of influence for our analysis (especially for the strengths of He II 4200 and 4541, respectively), we have run a number of simulations with different treatments of the He II resonance lines, for the example of our final model for HD 14947, where the majority of lines is formed in the wind. To check our hypothesis that the dominating effect leading to erroneous results follows from the increased pumping by resonance lines, two principally different approaches were considered, which should give similar results if the hypothesis were correct.

On the one hand, we set all He II resonance lines into detailed balance. Alternatively, we simulated an additional ρ-square dependent background opacity in the decisive frequency range 227 Å $< \lambda <$ 400 Å, defined by

$$\chi_\nu^{\rm add} = \kappa n_{\rm e} \cdot \rho \cdot f_\nu, \qquad (6)$$

with different values of κ between $3 \cdot 10^{-14}$ and $1 \cdot 10^{-16}$. The frequential dependence f_ν was assumed to be either increasing or decreasing,

$$f_\nu^1 = 1 - q_\nu$$
$$f_\nu^2 = 0.5(1 + q_\nu)$$

Table 5. Different approximations for treatment of He II resonance lines: The value of κ corresponds to the definition in Eq. (6), and the line styles are the same as in Figs. 24 and 26.

no.	approx.	κ	f_ν	line style
1	"standard"	–	–	dotted
2	detailed balance	–	–	dashed
3	blocked flux	$3 \cdot 10^{-14}$	f_ν^2	fully drawn
4	blocked flux	$3 \cdot 10^{-16}$	f_ν^1	dashed-dotted

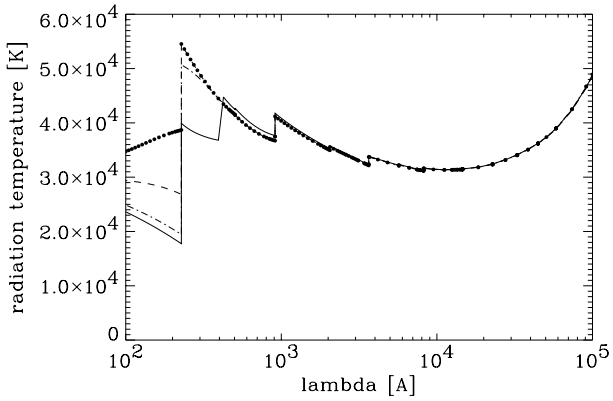

Fig. 24. Radiation temperatures of emergent fluxes for the model of HD 14947, with different treatment of He II resonance lines. Line styles as defined in Table 5.

$$q_\nu \;=\; \frac{1/\lambda - 1/227}{1/400 - 1/227}, \qquad (7)$$

and the appropriate emission component has been set to Planck. The value of κ corresponds to the inverse of the electron density at that point where the additional opacity reaches the same value as the electron scattering opacity. From the numbers given above, it is obvious that our choice is rather low compared to what might be expected in reality. For our final discussion, we have selected four models with parameters given in Table 5.

Fig. 24 verifies the expected behaviour for the He II ground-state. Both for the models with detailed balance as well as with simulated background opacities, He III begins to recombine in the outer atmosphere as long as the strong upward rates present in model 1 (dotted) are no longer active, so that a significantly enhanced ionization edge develops. Only for the model with the lowest value of $\kappa = 1{\cdot}10^{-16}$ (not displayed), the influence of the background opacity becomes so weak that the model remains ionized throughout the wind.

Besides the reaction of the ground-state, also the expected behaviour of the excited states (reversal of population) takes place as long as the radiation temperature does not significantly increase towards higher frequencies (model 3) or the resonance lines are not active (model 2). A comparison between the corresponding He II 4686 profiles and the observations (Fig. 25) shows that our simulations are in almost perfect agreement, whereas our standard model displays much too much emission. It is interesting to note here a remark given by our anonymous referee. Henrichs (1991) reports that the equivalent width of He II λ4686

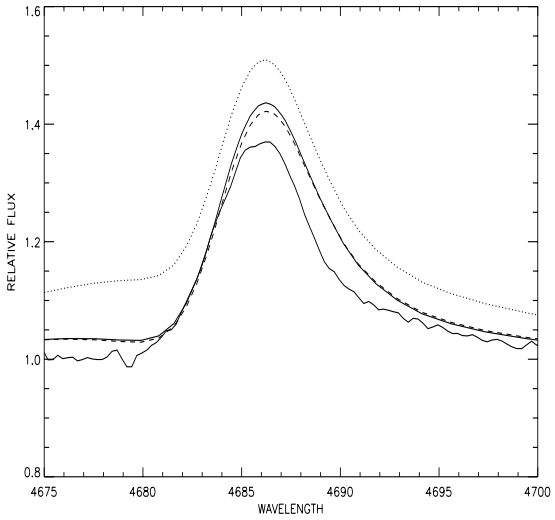

Fig. 25. Comparison of the He II 4686 profile observed in HD 14 947 with those obtained in our simulation of line–blocking (full drawn), of detailed balance for He II resonance transitions (dashed) and in our standard model (dotted).

in λCep varies in concert with the high–velocity edge of the C IV λ1550 line, suggesting that both variations share a common origin that could rely on the behaviour of the background opacity or the resonance lines of He II, as studied here.

A final check on how far our models compare to reality allows the comparison with the UV-line He II 1640 ($n = 2 \rightarrow 3$), since the lower state of this transition behaves differently from the other excited levels. In those cases where the resonance lines are no longer active (detailed balance) or are of negligible importance (background opacities) and the He II Lyman edge becomes optically thick throughout the atmosphere, this state becomes the effective ground state of the ion[4]. Thus, its population is predominantly controlled by the photoionization balance at 911 Å coinciding with the hydrogen Lyman edge. Since this edge is optically thin, the 2nd level becomes strongly overpopulated because of the diluted radiation field, i.e., the absorption should be larger than for the standard model. A comparison with the observed *IUE* profile[5] shows that our models are on the right track, in contrast to the standard model which predicts too little absorption. Only at higher velocities, i.e., in the outermost wind, are they too strong compared to observations, whereas for the inner wind, which is the decisive part concerning our analysis, they are in perfect agreement. A comparison with model 4 shows that some fine-tuning might improve even the situation at larger velocities. (We note that in order to fit the position of the emission peak, we had to apply an artificial velocity dispersion of roughly 100 km/s, consistent with the values found from the analysis of UV resonance lines.)

In conclusion, we found that suppressing the large upward rates from resonance lines present in our standard model gives

[4] This situation corresponds to the behaviour of H_α in A-type supergiants.

[5] SWP 10724, kindly provided in reduced form by I.D. Howarth and R.K. Prinja.

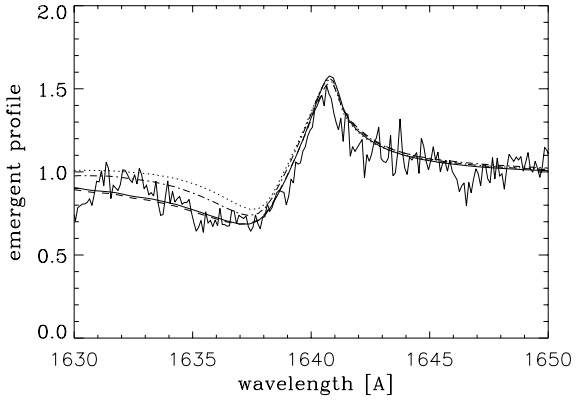

Fig. 26. *IUE* spectrum of HD 14947[5], He IIλ1640, compared to profiles generated from models with different treatment of He II resonance lines. Observations shifted by 90 km/s to the blue, velocity dispersion $v_{\rm turb}$ = 100 km/s applied to account for the red-shifted emission peak (see text). Line styles as defined in Table 5.

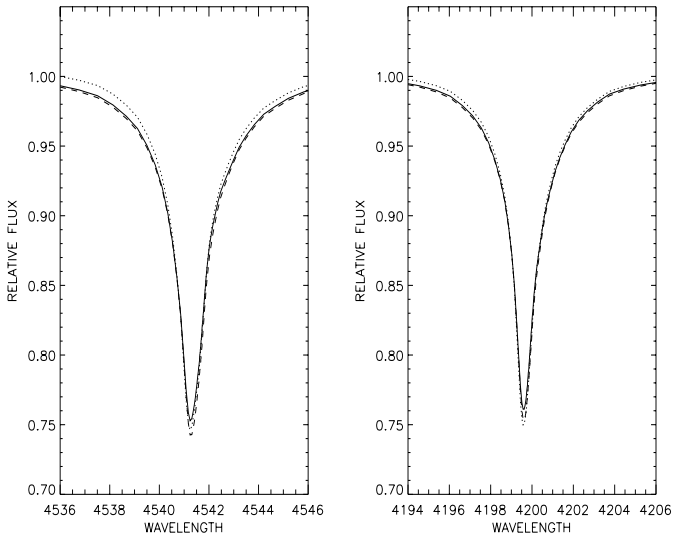

Fig. 27. Line profiles of He II 4541 (left) and He II 4200 (right) for the simulation of line-blocking (fully drawn), of detailed-balance (dashed), and for the "standard" model (dotted). Calculations were made for the final model of HD 14 947.

rise to a different population of ground and excited levels. The exact mechanism for this suppression, however, seems to be irrelevant to the results, and the synthesized profiles of previously problematic lines compare well with the observations.

We are now able to check the consequences of the manipulations outlined with respect to the strategic lines analysed so far and to derive constraints on which lines are more robust concerning our present ignorance of the real situation.

Fig. 27 shows the profiles of He II $\lambda\lambda$ 4541, 4200 produced by the different simulations and the "standard" model. We see that the wings of the He II lines become stronger in the simulations as a consequence of the now reduced departure coefficients of the upper levels. However, the effect is smaller in the He II λ4200 line (transition $4 \rightarrow 11$) than in the He II λ4541 (transition $4 \rightarrow 9$) because transitions involving higher levels are weaker and form closer to the photosphere, so that the increased source function is not so visible. Since He II 4200 shows up to be more stable, this is the preferred line in case of any discrepancy. This is a change of criterion with respect to former analyses in our group, but we prefer always to follow a single criterion that allows us to understand physically changes in the derived parameters. In addition, we should mention that also H_α becomes weaker, especially in the blue wing, as a consequence of these effects in the overlapping He II line. That is the reason why we prefer to fit the red wing in case of difficulties like those in λ Cep or HD 15 570 (and in concert with the findings by Puls et al. (1996), who had also to manipulate the He II departures predicted by unified models if the wind was strong). Finally, we point out that He I is not so strongly affected if these lines are formed purely in the photosphere, but, as has been shown by Santolaya–Rey et al. (1997) they are also influenced by any effects that modify the population of the He II ground level (see Sect. 3.4.1 in Santolaya–Rey et al., where this problem has already been discussed).

7. Discussion

The first thing which is evident from the spectral analysis is the increasing difficulty in fitting the spectra of the earliest types with plane–parallel model atmospheres. In particular, for 50 000 K and above we were unable to determine the stellar parameters in the same way as we did for stars in Paper I and for the rest of the objects in the present study. This is true even for the relatively large gravity star Cyg OB2 #7, and was nearly the case for the relatively cool star HD 15 558. Plane–parallel analyses are still useful, however, because they apply up to temperatures of 50 000 K and because they can be used as constraints for the analysis in the larger parameter space demanded by more sophisticated models.

The temperature scale defined by plane–parallel, hydrostatic, non-blanketed models is probably too hot (see Vacca et al. 1996; Harries & Hilditch 1998). For example, Hubeny et al. (1998) have shown that the same quality fit can be achieved for 10 Lac with a line-blanketed model at 35 000 K and with the non-blanketed model used in Paper I at 37 500 K (all other parameters remaining the same). The effect can be even larger for the stars analysed here, since the line-blocking effects in plane–parallel, hydrostatic models move the stars towards higher temperatures.

In the spherical, non-hydrostatic models we have used here, line-blocking has been simulated, and we have found that it has the same effect as to keep the He II resonance lines in detailed balance (which were already in detailed balance in the plane–parallel models, so that they did not show the influence on the He II lines of the Pickering series we observe in these spherical models). This effect had important consequences in our analyses. It led us to change the temperature criterion and adopt He II λ4200 as the main line for the fit, which resulted in lower temperatures than if we had adopted the He II λ4541 in those cases in which we could not fit both lines simultaneously. The sim-

Table 6. Γ values, terminal velocities and escape velocities (in km s^{-1}) obtained using the spectroscopic (sp) and evolutionary (ev) masses. In both cases we have taken into account the effect of the centrifugal force in reducing the escape velocity.

Star	V_∞	$\Gamma(sp)$	$\Gamma(ev)$	$v_{\rm esc}(sp)$	$V_\infty/\, v_{\rm esc}(sp)$	$v_{\rm esc}(ev)$	$V_\infty/\, v_{\rm esc}(ev)$
Cyg OB2 #7	2900	0.71	0.36	586	4.95	1231	2.36
HD 15 570	2600	0.31	0.43	1149	2.26	882	2.95
HD 15 629	3000	0.45	0.28	781	3.84	1148	2.61
HD 15 558	2800	0.46	0.43	981	2.85	1039	2.69
HD 14 947	2400	0.32	0.25	789	3.04	943	2.55
HD 210 839	2250	0.33	0.31	734	3.07	778	2.89
HD 5 689	2500	0.40	0.10	405	6.17	1013	2.47

ulations indicate that the reduction of the strong upward rates of the He II resonance lines (whatever the real physical cause) will help to bring both lines into agreement (although at the moment we cannot say whether it will bring them completely into agreement). It also suggested to us that we should fit the red wing of H_α whenever the fit to the whole line was impossible. What could be important for the future is that we have shown that He II λ4686 is also affected and its fit is highly improved (although still qualitatively) when the resonance lines of He II are kept in detailed balance, or the departure coefficient of the second level is kept below its detailed balance value through additional background opacity.

The plane–parallel spectroscopic masses are as usual lower than evolutionary masses (see Paper I or Vacca et al. 1996). The new temperature criterion does not strongly influence the mass discrepancy. In Paper I we showed that lowering the temperature (for whatever reason) will not bring the masses into agreement. In the present case, however, we find the mass discrepancy even for luminosity class V stars. This finding is contrary to the conclusion we obtained in Paper I (and is in agreement with other authors; see, for example, Vacca et al. 1996), namely that luminosity class V stars do not show a mass discrepancy. The reason for this apparent contradiction is that the gravities we derive here are also low for these luminosity class V stars. Thus the conclusion should be rather that 'high-gravity stars do not show a mass discrepancy,' where the term 'high' actually depends on the strength of the radiation field.

This indicates a problem of the hydrostatic models due to the intense radiation pressure, and in fact larger gravities are derived when using the spherical models with mass-loss, largely reducing the mass discrepancy, which is now about 50%. This result is even reinforced when we realize that most temperatures are now lower due to sphericity and a new temperature indicator. An additional contribution came in some cases from the fact that the wings of H_γ can be strongly affected by wind contamination. In one case (HD 15 570) this contamination is so strong that actual information about the gravity from the wings of H_γ is lost. In all other cases, however, the systematic effect that spectroscopic masses (without line-blanketing or blocking) are lower than evolutionary ones (without mixing mechanisms) is still present (note that formally the error bars overlap, and it is only because the effect is systematic that we can speak of a mass discrepancy).

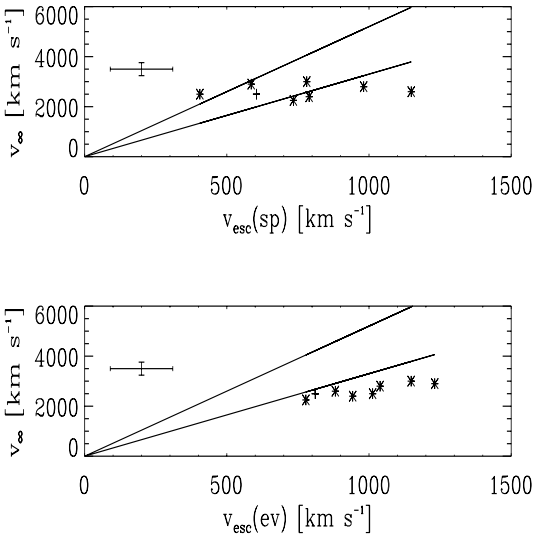

Fig. 28. The escape velocities obtained from spectroscopic (above) and evolutionary (below) masses, against the wind terminal velocities, all in km s^{-1}. The lines have the slopes predicted by theory for α values of 0.6 and 0.7, e.g., 3.3 and 5.2. Plus signs mark the position of HD 5 689 if this star is assigned a magnitude of –5.78, typical of a O6 III star. Typical error bars have been plotted in the upper right corner. The abscissa error of Cyg OB2#7 in the upper plot is twice the corresponding error bar, due to its high $\Gamma(sp)$ value

The problem can be alternatively formulated using the escape velocities. (Table 6 gives the escape velocities and related values). Escape velocities have been derived using $\log g$ values uncorrected for centrifugal forces, i.e., the *measured* values implicitely including the centrifugal force acceleration (cf. Sect. 4) which determine the *effective* escape velocities.

Fig. 28 shows the correlation between escape velocities and terminal wind velocities. We see that the diagram using evolutionary masses shows a good linear correlation between both quantities, whereas that with the spectroscopic masses shows a weaker correlation. However, the last diagram is in better agreement with the theory of radiatively driven winds. This theory predicts for the O-star domain (i.e., if the force-multiplier parameter δ is small, cf. Friend & Abbott 1986; Kudritzki et al.

1989)

$$v_\infty \simeq 2.24 \frac{\alpha}{1-\alpha} v_{\rm esc},$$

with $v_{\rm esc}$ the escape velocity and α one of the line force multiplier parameters (the coefficient in the exponent of the line strength distribution function). With typical values for OB stars of α= 0.6–0.7 we obtain values of 3.3–5.2 for the ratio of terminal-to-escape velocity. This range of values is in agreement with those found here for the spectroscopic masses (see Table 6; note that the only point deviating from this range corresponds to HD 15 570, whose gravity and spectroscopic mass are very uncertain, and that HD 5 689, which is the leftmost point in the upper part of Fig. 28, would lie in the middle of the range if the absolute magnitude of a luminosity class III object were assumed).

On the other hand, we derive very low ratios between terminal and escape velocities when using evolutionary masses (see Table 6), with an average ratio of 2.57, corresponding to α= 0.53 (which would be very low for the considered spectral range). Thus, Fig. 28 seems to indicate that the evolutionary masses are *systematically* too large (via the corresponding escape velocities), whereas the spectroscopic ratios are closer to the theoretically expected range. In Fig. 29 we can see this result, already contained in former papers (Groenewegen et al. 1989; Lamers & Leitherer 1993), from a slightly different point of view. Here we have plotted the ratio of evolutionary-to-spectroscopic mass versus the ratio of spectroscopic-to-evolutionary α. We see that, except for the odd case HD 5 689, there is a strong correlation, indicating the relation between mass discrepancy and our present knowledge of radiatively driven winds. (Note moreover that HD 5 689 would perfectly fit into the correlation when an absolute magnitude of -5.78 is assumed, as appropriate for an O6 III star, but note also that the terminal velocity for this star was derived from the spectral type–terminal velocity relation from Haser 1995, as was that of Cyg OB2#7). We should stress that we adopt a β–law for the wind velocity and determine then the α's directly from the derived relation between $V_\infty$and escape velocity. Thus the agreement of the spectroscopic α's with the predictions of the radiatively driven wind velocity results in mutual support.

At present it is still unclear whether the inconsistency found is due to some physical effects that should be incorporated into the evolutionary or into the atmospheric models, although the former are perfectly able to explain the discrepancy, at least qualitatively, when introducing mixing effects (Heger 1998) that could also affect surface abundances.

Spherical models with mass-loss do not contribute to reduce the helium abundances found with plane–parallel models. In previous analyses (Herrero et al. 1995; Israelian et al. 1999) in which we used He I $\lambda\lambda$4387, 4922 and He II λ4541 as temperature indicators, the derived helium abundances were similar. As a result of the new indicator, the helium abundances had now to increase. However, we see that the stars of larger gravity (HD 15 558 and HD 15 629) do not seem to show He overabundances. Normal supergiants lie between the former and the fast rotators, that show the largest overabundances, in agreement

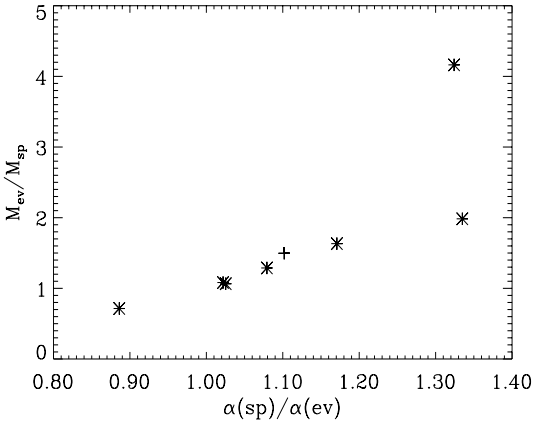

Fig. 29. The ratio α(sp)/α(ev) against the mass ratio $M_{\rm ev}/M_{\rm s}$. Asterisks refer to the values quoted in Table 3 (in particular, the asterisk in the upper right corner corresponds to HD 5 689), whereas the cross marks the position of HD 5 689 if this star is assigned a magnitude of –5.78, typical of an O6 III star.

with results from Paper I and the possibility that rotation plays a fundamental role in the chemical evolution of single stars. However, it is not clear whether a difference exists in the mass discrepancy between the rapid rotators and the other stars, or a correlation between the mass and helium discrepancies, that could indicate an overluminous evolution, as predicted by evolutionary rotating models (see Langer & Heger 1998, Maeder 1998 or Meynet 1998 and references therein). We should stress here that we do not consider HD 5 689 as really showing such a large mass discrepancy as it appears to do in Tables 2 and 3, but that it is a problem of the stellar classification (or a problem of assigning the star to the Cas OB7 association).

Derivation of the mass–loss rates has been hindered by our finding of the inconsistency between H_α and H_γ in those cases in which the wind is particularly strong. Thus we have found that both lines can demand mass–loss rates that differ up to a factor of two. We prefer the values given by H_α because it is more sensitive to mass-loss, and attribute the problem to difficulties in describing the wind in the transition zone. IR observations and analyses giving information about this zone should help in the future to solve the problem.

From the three stars for which we had some information about mass–loss rates derived from radio emission, only one (for which in addition only an upper limit from radio fluxes is available) shows agreement between the H_α and radio values. For the other two, radio mass–loss rates are a factor of three to four lower than H_α mass–loss rates (and thus H_γ values would be in between). However, several facts should be taken into account before claiming that there is a contradiction between both sets of values. First, the concerned stars are only two particular, rather special cases (one, HD 15 570, is a very extreme O star, and the other, HD 210 839, is a strong non-radial pulsator, rapid rotator with a probably non–spherically symmetric wind, cf. Sect. 5.2); secondly, what we actually obtain from the observations are Q values, proportional to $(\dot{M}/({\rm R v}_\infty)^{3/2})$ for H_α, and to $(\dot{M}/({\rm R}^{3/2}{\rm v}_\infty))$ for radio and thus the derived values depend

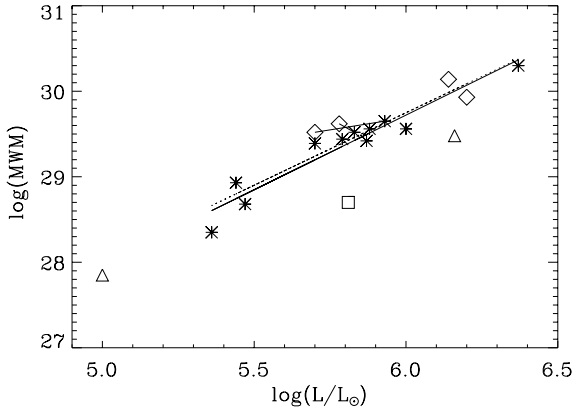

Fig. 30. The wind momentum–luminosity relation for the stars in our sample. The abcissa is $\log(L/L_{\odot})$ and the ordinate is the logarithm of the modified wind momentum (MWM), log ($\dot{M}\ V_{\infty}R^{0.5}$). Asterisks represent OB supergiants from Puls et al. (1996). Open diamonds, squares and triangles are respectively OB supergiants, giants and dwarfs from the present work. The positions of HD 14 947 and HD 210 839 in both studies are joined by a line, where the major difference results from the different effective temperatures and helium-abundances attributed to the objects.

on the particular set of chosen stellar parameters; and thirdly, also the proportionality constants in the case above depend on model details (for example, Lamers & Leitherer 1993, assume that He is doubly ionized in the wind of HD 210 839 between 10 and 100 stellar radii, whereas our calculations indicate that from 28 stellar radii upwards, He is single ionized, which would have an immediate effect on the derived radio mass–loss rates, increasing them). Thus, we cannot state that there is a general problem (or even a particular one), or decide which value we should prefer for each object.

Having derived all parameters we can obtain the modified wind momenta of all stars for which the radiation-driven wind predicts a tight correlation with luminosity. Our results are given in Table 3 and plotted in Fig. 30, together with the data given by Puls et al. (1996) for Galactic supergiants. We see that our points for supergiants agree well with theirs (we have discussed the differences in the individual studies). We have also plotted the regression lines derived from the supergiants from Puls et al. and from all the supergiants (the former and ours) to stress this point. We see that both regression lines are quite parallel, indicating that the new values do not significantly change the known WLR.

8. Conclusions and future work

We have presented the spectra of seven Galactic luminous O stars, that have been analysed by means of non-LTE, plane–parallel, hydrostatic model atmospheres, including line-blocking, and by means of spherical, mass-losing models. We have used these analyses to study some additional effects (physical as well as due to applied approximations) that have an influence on the results.

We have shown that line-blocking has to be taken into account when analysing very hot stars, in plane–parallel as well as in spherical models with mass-loss. Line-blocking indirectly affects the spectral-line diagnostics through changes in the level populations of He. Although for the spherical models with mass-loss we only made simulations, this is clearly one direction for future model improvements. In particular, we obtained very interesting results concerning the He II λ4686 line and the blue wing of H_{α} (actually, concerning the corresponding He II blend).

One of the conclusions of the present paper is that around 50 000 K (the exact value depending on gravity) we reach the limit of applicability of plane–parallel, hydrostatic models to real massive stars. This conclusion can be further refined, if we take into account the fact that line-blanketed models could give lower temperatures, or if we consider that spherical models with mass-loss will demand larger gravities. The final result would be models less affected by radiation pressure, larger masses and a cooler temperature scale.

Spherical models with mass-loss are thus needed to analyse these stars. We had to correct the gravities of all stars (except HD 5 689) when using these models, sometimes with increments as large as 0.25 dex. Part of the differences in the stellar parameters derived from both sets of models are due to a change in the preferred temperature indicator.

Our spherical models with mass-loss are also still not free from internal inconsistencies. For some models with strong winds, we see that He II $\lambda\lambda$4200, 4541 give different temperatures, although we expect that inclusion of line-blocking will reduce this discrepancy, and will strongly improve the fits of He II λ4686 and the blue wing of H_{α}. We have also found that for stars with strong winds there is a difference in the mass–loss rates derived from H_{α} and H_{γ}, that can reach a factor of two. We do not find good agreement with the two cases for which we have mass–loss rates from radio fluxes, although it is not possible to derive any firm conclusion from this fact.

The helium and mass discrepancies found here are in agreement with the findings of Paper I. The only difference is that we find a mass discrepancy also for luminosity class V stars, but this is actually misleading. What we find is that the luminosity class V stars analysed here have gravities lower than usual for their spectral classification. The conclusion of Paper I should then be changed to state that we do not find the mass discrepancy for stars with high gravities. At least a part of this effect is attributed to the fact that the intense radiation field affects the wings of the Balmer lines also for these stars. An additional possibility is that they actually never reach the zero-age main sequence (see, for example, Hanson 1998).

Spherical models with mass-loss largely reduce the mass discrepancy. Without solving it completely, the problem lies now in the systematic trend of spectroscopic values to be lower than evolutionary ones, but most of the individual values now agree within the formal error bars. We have also shown that the spectroscopic masses agree better with the predictions from the radiatively driven wind theory, because they give ratios of the terminal wind velocity to the escape velocity (or equiva-

lently, values of the α line force parameter) that are in the range predicted by that theory.

From the point of view of individual stars, we have analysed some of the most massive and luminous stars in the Milky Way. We have found that three of them (Cyg OB2 #7, HD 15 570 and HD 15 558) have particularly large initial masses, around or in excess of 100 $M_\odot$ (depending on the technique used for the mass derivation). Cyg OB2#7, HD 14 947 and HD 210 839 have so extreme mass–loss rates that the wings of H_γ are strongly affected, and in HD 15 570 the wind is so strong that the exercise of deriving the gravity from the wings of H_γ results in highly uncertain values. On the other hand, we find that HD 5 689, the less luminous object in our sample, could have been wrongly assigned to Cas OB7, and might be a runaway star.

Acknowledgements. We would like to thank our anonymous referee for many valuable comments and suggestions. AH wants to acknowledge support for this work by the spanish DGES under project PB97-1438-C02-01.

References

Auer L.H., Mihalas D., 1972, ApJS 24, 193
Blaauw A., 1993, In: Cassinelli J.P., Churchwell E.B. (eds.) Massive Stars: their lives in the interstellar medium. ASP Conf. Series Vol. 35, p. 207
Conti P.S., Ebbets D., 1977, ApJ 213, 438
Conti P.S., Frost S.A., 1977, ApJ 212, 728
Conti P.S., Hanson M.M., Morris P.W., Willis A.J., Fossey S.J., 1995, ApJ 445, L35
de Jong J.A., Henrichs H.F., Schrijvers C., et al., 1999, A&A 345, 172
de Koter A., 1998, In: Howarth I.D. (ed.) II Boulder–Munich Workshop on Properties of Hot, Luminous Stars. ASP Conf. Series Vol. 131, p. 343
Feldmeier A., Puls J., Pauldrach A.W.A., 1997, A&A 322, 878
Friend D.B., Abbott D.C., 1986, ApJ 311, 701
Fullerton A.W., Gies D.R., Bolton C.T., 1996, ApJS 103, 475
Gabler R., Gabler A., Kudritzki R.P., Puls J., Pauldrach A.W.A., 1989, A&A 226, 162
Garmany C.D., Stencel R.E., 1992, A&AS 94, 211
Garmany C.D., Vacca W.D., 1991, PASP 103, 347
Groenewegen M.A.T., Lamers H.J.G.L.M., Pauldrach A.W.A., 1989, A&A 221, 78
Hanson M.M., 1998, In: Howarth I.D. (ed.) II Boulder–Munich Workshop on Properties of Hot, Luminous Stars. ASP Conf. Series Vol. 131, p. 1
Harries T.J., Hilditch R.W., 1998, In: Howarth I.D. (ed.) II Boulder–Munich Workshop on Properties of Hot, Luminous Stars. ASP Conf. Series Vol. 131, p. 401
Haser S.M., 1995, Ph.D. Thesis, Universitäts–Sternwarte der Ludwig–Maximillian Universität, München
Heger A., 1998, Ph.D. Thesis, Technische Universität München
Henrichs H., 1991, In: Baade D. (ed.) Proc. of the ESO workshop on Rapid variability of OB stars, Nature and diagnostic value. ESO Conference and Workshop Proceedings Vol. 36, p. 191
Herrero A., 1994, Space Sci. Rev. 66, 137
Herrero A., Vílchez J.M., Kudritzki R.P., 1990, In: Garmany C.D. (ed.) I Boulder–Munich Workshop on Intrinsic Properties of Hot, Luminous Stars. ASP Conf. Series Vol. 7, p. 50
Herrero A., Kudritzki R.P., Vílchez J.M., et al., 1992, A&A 261, 209 (Paper I)
Herrero A., Kudritzki R.P., Gabler R., Vílchez J.M., Gabler A., 1995, A&A 297, 556
Herrero A., Corral L.J., Villamariz M.R., Martín E.L., 1999, A&A 348, 542
Howarth I.D., 1998, In: Howarth I.D. (ed.) Proceedings of the II Boulder–Munich Workshop on Properties of Hot, Luminous Stars. ASP Conf. Series Vol. 131
Howarth I.D., Siebert K.W., Hussain G.A.J., Prinja R.K., 1997, MNRAS 284, 265
Hubeny I., Heap S.R., Lanz T., 1998, In: Howarth I.D. (ed.) II Boulder–Munich Workshop on Properties of Hot, Luminous Stars. ASP Conf. Series Vol. 131, p. 108
Humphreys R.M., 1978, ApJS 38, 309
Israelian G., Herrero A., Musaev F., et al., 1999, MNRAS, submitted
Kiriakidis M., Fricke K.J., Glatzel W., 1993, MNRAS 264, 50
Kudritzki R.P., 1980, A&A 85, 174
Kudritzki R.P., Hummer D.G., 1990, ARA&A 28, 303
Kudritzki R.P., Simon K.P., Hamman W.R., 1983, A&A 118, 245
Kudritzki R.P., Pauldrach A.W.A., Puls J., Abbott D.C., 1989, A&A 219, 205
Lamers H.J.G.L.M., Leitherer C., 1993, ApJ 412, 771
Lang K.R., 1980, Astrophysical Formulae. 2nd edition, Springer Verlag, p. 531
Langer N., Heger A., 1998, In: Howarth I.D. (ed.) II Boulder–Munich Workshop on Properties of Hot, Luminous Stars. ASP Conf. Series Vol. 131, p. 76
Maeder A., 1998, In: Howarth I.D. (ed.) II Boulder–Munich Workshop on Properties of Hot, Luminous Stars. ASP Conf. Series Vol. 131, p. 85
Mason B.D., Gies D.R., Hartkopf W.I., et al., 1998, AJ 115, 821
Massey P., Thompson A.B., 1991, AJ 101, 1408
Matthews T.A., Sandage A.R., 1963, ApJ 138, 30
Meynet G., 1998, In: Howarth I.D. (ed.) II Boulder–Munich Workshop on Properties of Hot, Luminous Stars. ASP Conf. Series Vol. 131, p. 96
McErlean, N.D., Lennon, D.J., Dufton P.L. 1998, A&A 329, 613
Najarro F., Kudritzki R.P., Hillier D.J., et al., 1998, In: Howarth I.D. (ed.) II Boulder–Munich Workshop on Properties of Hot, Luminous Stars. ASP Conf. Series Vol. 131, p. 57
Owocki S.P., Gayley K.G., Cranmer S.R., 1998, PASPC 131, 237
Pauldrach A.W.A., Kudritzki R.P., Puls J., Butler K., Hunsinger J., 1993, A&A 283, 525
Penny L.R., 1996, ApJ 463, 737
Petrenz P., Puls J., 1996, A&A 312, 195
Puls J., Kudritzki R.P., Herrero A., et al., 1996, A&A 305, 171
Santolaya–Rey A.E., Puls J., Herrero A., 1997, A&A 488, 512
Schaerer D., Schmutz W., 1994, A&A 288, 231
Schaller G., Schaerer D., Meynet G., Maeder A., 1992, A&AS 96, 269
Schmutz W., 1997, A&A 288, 231
Sellmaier F., 1996, Thesis, Ludwig-Maximilian-Universität München
Smith K.C., Howarth I.D., 1998, MNRAS 299,1146
Taresch G., Kudritzki R.P., Hurwitz M., et al., 1997, A&A 321, 531
Vacca W.D., Garmany C.D., Shull J.M., 1996, ApJ 460, 914
Voels S.A., Bohannan B., Abbott D.C., Hummer D.G., 1989, ApJ 340, 1073
Walborn N.R., 1972, AJ 77, 312
Walborn N.R., 1973, AJ 78, 1067